

UNIVERSIDAD SAN FRANCISCO DE QUITO USFQ

Colegio de Ciencias e Ingeniería

Application of group theory methods for
the synthesis of quantum operators in low
dimensional materials.

Juan Esteban Zurita Lema

Física

Trabajo de titulación presentado como requisito
para la obtención del título de

Licenciado en Física

May 20, 2024

UNIVERSIDAD SAN FRANCISCO DE QUITO USFQ

Colegio de Ciencias e Ingeniería

HOJA DE CALIFICACIÓN DE TRABAJO DE FIN DE
CARRERA

Juan Esteban Zurita Lema

Nombre del profesor, Título académico: Ernesto Medina Dagger, PhD

May 20, 2024

© Derechos de Autor

Por medio del presente documento certifico que he leído todas las Políticas y Manuales de la Universidad San Francisco de Quito USFQ, incluyendo la Política de Propiedad Intelectual USFQ, y estoy de acuerdo con su contenido, por lo que los derechos de propiedad intelectual del presente trabajo quedan sujetos a lo dispuesto en esas Políticas.

Asimismo, autorizo a la USFQ para que realice la digitalización y publicación de este trabajo en el repositorio virtual, de conformidad a lo dispuesto en la Ley Orgánica de Educación Superior del Ecuador.

Nombres y apellidos: Juan Esteban Zurita Lema

Código: 00327058

Cédula de Identidad: 1723871933

Lugar y fecha: May 20, 2024

ACLARACIÓN PARA LA PUBLICACIÓN

Nota: El presente trabajo, en su totalidad o cualquiera de sus partes, no debe ser considerado como una publicación, incluso a pesar de estar disponible sin restricciones a través de un repositorio institucional. Esta declaración se alinea con las prácticas y recomendaciones presentadas por el Committee on Publication Ethics COPE descritas por Barbour et al. (2017) Discussion document on best practice for issues around theses publishing, disponible en <http://bit.ly/COPETheses>

UNPUBLISHED DOCUMENT

Note: The following capstone project is available through Universidad San Francisco de Quito USFQ institutional repository. Nonetheless, this project – in whole or in part – should not be considered a publication. This statement follows the recommendations presented by the Committee on Publication Ethics COPE described by Barbour et al. (2017) Discussion document on best practice for issues around theses publishing available on <http://bit.ly/COPETheses>

Agradecimientos

A Ernesto Medina por su gran apoyo y guía. A Melissa Infussino, Silvana Guitarra y César Zambrano por la Beca Arquímedes. A mis padres, Natalia y Juan Carlos, por ser mi hogar. A mi hermana Carla, por ser mi mejor amiga, creer en mí y acompañarme siempre, aunque estemos lejos.

Resumen

En este trabajo, se utiliza el enfoque de expansión invariante para determinar el Hamiltoniano de las subredes de grafeno consistente con los elementos de simetría del grupo puntual D_{3h} . El estudio incluye los efectos del momento, el pseudospín y los términos activos de espín. Inicialmente, el Hamiltoniano se genera utilizando el método de enlace fuerte, hasta el tercer orden alrededor del punto de alta simetría \mathbf{K} de Dirac. Posteriormente, el mismo Hamiltoniano se deriva utilizando el enfoque teórico de grupos. Se explican varios conceptos de la teoría de grupos, con ejemplos proporcionados para ayudar al lector a familiarizarse con el formalismo de expansión invariante. El principal producto de este trabajo es un software desarrollado para generar operadores Hamiltonianos para un grupo puntual arbitrario. El análisis resalta las principales deficiencias de los enfoques de enlace fuerte y teóricos de grupos en la derivación de Hamiltonianos modelo efectivos, y muestra cómo combinarlos para describir materiales de manera exitosa.

Palabras clave: *expansión invariante, enlace fuerte, grupo puntual D_{3h}*

Abstract

In this work, the invariant expansion approach is utilized to determine the Hamiltonian for graphene sublattices consistent with the symmetry elements of the point group D_{3h} . The study includes the effects of momentum, pseudospin, and spin active terms. Initially, the Hamiltonian is generated using the tight-binding method, up to third order around the high symmetry \mathbf{K} Dirac point. Subsequently, the same Hamiltonian is derived using the group theoretical approach. Several concepts of group theory are explained, with examples provided to help the reader familiarize themselves with the invariant expansion formalism. The main product of this work is software developed to generate Hamiltonian operators for an arbitrary point group. The analysis highlights key shortcomings of both the tight-binding and group theoretical approaches in deriving effective model Hamiltonians, and shows how to combine them to successfully describe materials.

Keywords: *invariant expansion, tight binding, D_{3h} point group*

Contents

1	Introduction	12
1.1	The Tight Binding Model in Graphene	13
1.2	Transfer and Overlap Integrals	18
1.2.1	Hamiltonian and overlap matrix elements	18
1.2.2	Phase factors	21
1.3	Eigenvalue equation	22
1.4	Spin-Orbit Coupling Hamiltonian	25
1.5	Adding new physics systematically	27
2	Methods	29
2.1	Principles of theory of invariants	30
2.2	Symmetry operations in D_{3h}	33
2.3	Symmetry elements acting on the operator \mathcal{K}	34
2.4	Character tables	38
2.5	Reducible Representations and Hamiltonians	40
3	Results	44
3.1	Invariant expansion at A and B sublattices	44
3.2	<i>No-go</i> SOC matrix elements	48
3.3	Software Development	50

	8
4 Conclusions	52
Bibliografia	53
5 Annexes	57
Annex A Nearest neighbors on graphene	57
Annex B Eigenvectors for Graphene	59
Annex C Physical constants for TB and SOC block Hamiltonian	60
Annex D Matrix representations for symmetry elements in D_{3h}	61
Annex E Reduction of $\Gamma_5 \otimes \Gamma_5^*$	62
Annex F Invariant expansion details	63
Annex G Code for analytic calculations	65

List of Tables

2.1	Character Table for D_{3h} point group and $D_{3h}(M)^2$ double group ¹	38
2.2	Reducible Direct Products for D_{3h}	42
3.1	Expansion parameters for momentum \mathbf{k} and spin \mathbf{s}	45
5.1	Matrix representations for elements in D_{3h}	61
5.2	Reducción de representación $\Gamma_{\bar{5}} \otimes \Gamma_{\bar{5}}^*$	62

List of Figures

- 1.1 (a) The primitive lattice vectors on the honeycomb crystal structure of monolayer graphene. The shaded rhomb is a unit cell with atoms A and B, one of each sub-lattice. (b) The reciprocal lattice vectors. The coloured hexagon represents the first Brillouin zone. Both Dirac valleys \mathbf{K} and \mathbf{K}' are displayed. 14
- 1.2 First K -nearest neighbors around carbon a B atom in graphene lattice: (a) nearest-neighbors, (b) next nearest-neighbors, (c) next next nearest-neighbors. 16
- 1.3 (a) Bands at points of high symmetry at the edge of the first Brillouin zone. (b) Energy surfaces around Dirac points². 25
- 2.1 Standard axis and atom labeling convention for pristine graphene. 33
- 2.2 Symmetry operations of graphene sub-lattices: (a) axes of proper rotation, and (b) planes of reflection. The shaded plane is one of the three vertical reflection planes σ_v , while the graphene plane is the horizontal reflection σ_h 34

2.3	D_{3h} symmetry operations on graphene. The figures show atoms in the B sublattice switching positions with respect to the identity element E . The vector \mathbf{z} is green when the operation switches the direction of the plane. The original system of reference in blue is left for reference.	35
3.1	Diagrams for <i>no-go</i> rules. Notice that the first rule at (a) applies for any pair of sites on the lattice. The second and third rules (b) only consider the first-nearest neighbors.	49
3.2	Flow chart for the use of the software to generate an invariant expansion of a Hamiltonian operator, using group theory.	51
5.1	UML diagram for <i>BlockHamiltonian</i> and <i>PointGroup</i> classes.	65
5.2	UML diagram for <i>SymmetryOperation</i> and <i>MathTools</i> classes.	66

Chapter 1

Introduction

Tight-binding (TB) models provide an effective, though not systematic, way to predict how electrons behave in solids by allowing the choice of an arbitrary number of neighbors to describe the physics of a material. They are especially useful for understanding materials with complex band structures, like graphene, and help explain special features such as the linear dispersion at the Fermi level^{3,4}.

However, any perturbation added to the TB Hamiltonian is usually considered with highly informed criteria, which can lead to the exclusion of important terms, failing to explain significant physical processes. While these omissions are often negligible in materials with relatively light atoms like graphene³, more complex systems do not follow this trend.

An alternative approach utilizes group theory tools to synthesize Hamiltonians by exploiting the symmetries of materials, known as invariant expansion. This

method determines which point group best describes a material and selects a basis set of wave functions that characterize the properties of the electrons, resulting in a Hamiltonian described by a reducible representation of the point group.

The main advantage of this approach is its focus on the macroscopic characteristics of the material, in contrast to TB models, which are often considered a microscopic approach to solid-state physics. This perspective provides a clearer understanding of the overall physical system, which is usually lost when using the TB approach^{3,5}.

The primary purpose of this work is to develop tools to generalize the ideas of invariant expansion to other physical systems, using graphene as a model. The ultimate goal is to establish a foundation for describing electron transport in low-dimensional materials.

1.1 The Tight Binding Model in Graphene

The primitive lattice vectors \mathbf{a}_1 and \mathbf{a}_2 of the Bravais lattice in Cartesian coordinates are shown in Figure 1.1a. The parameter $a = 2.46 \text{ \AA}$ ⁶ is the distance between two atoms of the sub-lattice A or B ^{3,7}.

$$\mathbf{a}_1 = a(1, 0), \quad \mathbf{a}_2 = a\left(\frac{1}{2}, \frac{\sqrt{3}}{2}\right) \quad (1.1)$$

The primitive reciprocal lattice vectors \mathbf{b}_1 and \mathbf{b}_2 (1.2) are obtained using the relation $\mathbf{a}_i \cdot \mathbf{b}_j = 2\pi\delta_{ij}$. These form the reciprocal lattice shown in Figure 1.1b.

$$\mathbf{b}_1 = \frac{2\pi}{a} \left(1, -\frac{1}{\sqrt{3}} \right), \quad \mathbf{b}_2 = \frac{2\pi}{a} \left(0, \frac{2}{\sqrt{3}} \right) \quad (1.2)$$

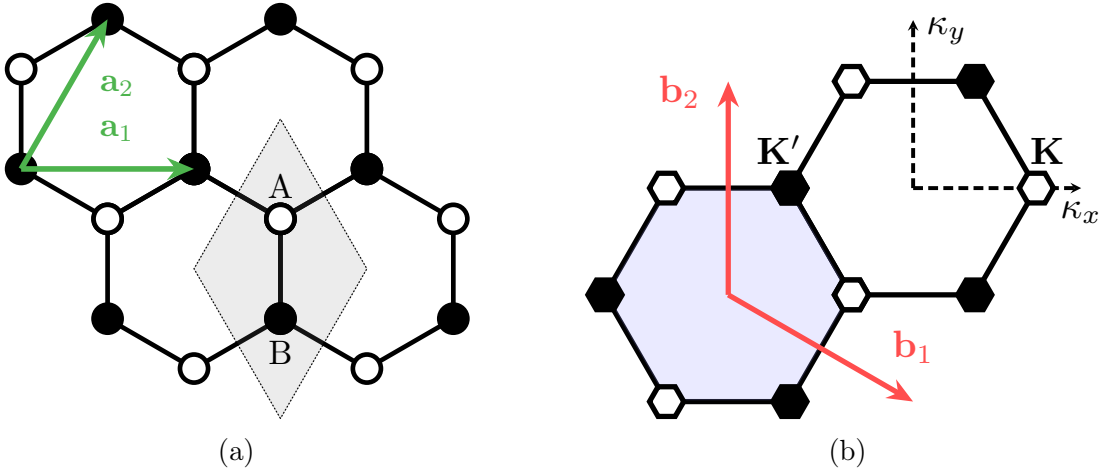


Figure 1.1: (a) The primitive lattice vectors on the honeycomb crystal structure of monolayer graphene. The shaded rhomb is a unit cell with atoms A and B, one of each sub-lattice. (b) The reciprocal lattice vectors. The coloured hexagon represents the first Brillouin zone. Both Dirac valleys \mathbf{K} and \mathbf{K}' are displayed.

Since the dispersion relation in the π electrons of graphene is independent of the rest of the eigenvalues of the Hamiltonian, the energy bands can be approximated by a TB model to an arbitrary number of nearest-neighbors^{6,8}. For this work, we choose to use third nearest neighbors to provide a general description of the system, from which we can study simplifications or extend the analysis for more generality as needed.

The normalized Bloch electronic wave function (1.3) for the carbon p_z orbitals in the \mathbf{K} Dirac valley consists of a linear combination of Bloch functions that use

coefficients $c_{\lambda n}(\boldsymbol{\kappa})$, and a π -orbital function $\Phi_{\lambda\boldsymbol{\kappa}}(\mathbf{r})$ that contains phase components dependent on atom position vectors \mathbf{R}_λ on each sublattice $\lambda = A, B$, which correspond to the two atomic wavefunctions in the unit cell, as seen in Figure 1.1a^{3,6}. The summations extend over all N unit cells within the lattice.

$$\Psi_{\boldsymbol{\kappa}n}(\mathbf{r}) = \sum_{\lambda} c_{\lambda n}(\boldsymbol{\kappa}) \Phi_{\lambda}(\mathbf{r}) \quad (1.3)$$

$$\Phi_{\lambda}(\mathbf{r}) = \frac{1}{\sqrt{N}} \sum_{\mathbf{R}_\lambda} e^{i\boldsymbol{\kappa} \cdot \mathbf{R}_\lambda} \phi_{\lambda}(\mathbf{r} - \mathbf{R}_\lambda) \quad (1.4)$$

First, second, and third nearest neighbors for an atom in the unit cell are defined by equations (1.5) to (1.7), respectively. Notice that in all cases, the symmetry of the system allows to obtain all vectors by a rotation matrix $\mathcal{R}(\theta)$ ³. The complete sets of vectors are mentioned in Annex A.

$$\boldsymbol{\tau}_1^{(j)} = \mathcal{R}(2j\pi/3)\boldsymbol{\tau}_1^{(3)}, \quad j = 1, \dots, 3, \quad \boldsymbol{\tau}_1^{(3)} = a \left(0, \frac{1}{\sqrt{3}} \right) \quad (1.5)$$

$$\boldsymbol{\tau}_2^{(j)} = \mathcal{R}(j\pi/3)\mathbf{a}_1, \quad j = 1, \dots, 6 \quad (1.6)$$

$$\boldsymbol{\tau}_3^{(j)} = \mathcal{R}(2j\pi/3)\boldsymbol{\tau}_3^{(3)}, \quad j = 1, \dots, 3, \quad \boldsymbol{\tau}_3^{(3)} = a \left(0, -\frac{2}{\sqrt{3}} \right) \quad (1.7)$$

Electron mobility is influenced by interactions among sites within the lattice. The most general form of the energy of the j -th band, using its eigenbasis $|\Psi_j\rangle$, is given by Equation 1.8⁶. Bands span over n atomic wavefunctions in the unit cell $j = 1, 2, \dots, n$. The Hamiltonian matrix elements $\mathcal{H}_{ij} = \langle \Phi_i | \hat{\mathcal{H}} | \Phi_j \rangle$ and overlap matrix elements $\mathcal{S}_{ij} = \langle \Phi_i | \Phi_j \rangle$ appear in the expansion. The coefficients c_{ij}^* are

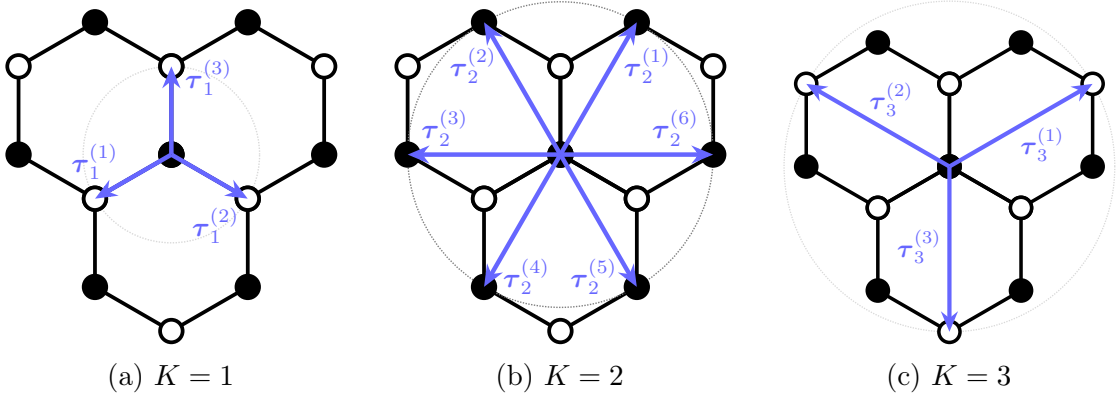


Figure 1.2: First K -nearest neighbors around carbon a B atom in graphene lattice: (a) nearest-neighbors, (b) next nearest-neighbors, (c) next next nearest-neighbors.

also functions of the momentum vector $\boldsymbol{\kappa}$, therefore are determined for each $\boldsymbol{\kappa}$ ⁶.

$$\epsilon_j(\boldsymbol{\kappa}) = \frac{\langle \Psi_j | \hat{\mathcal{H}} | \Psi_j \rangle}{\langle \Psi_j | \Psi_j \rangle} = \frac{\sum_{i,l} c_{ji}^* c_{jl} \langle \Phi_i | \hat{\mathcal{H}} | \Phi_l \rangle}{\sum_{i,l} \mathcal{S}_{il} c_{ji}^* c_{jl}} \quad (1.8)$$

$$\frac{\partial \epsilon_j}{\partial c_{jm}^*} = \frac{\sum_l \mathcal{H}_{ml} c_{jl}}{\sum_{i,l} c_{ji}^* c_{jl} \langle \Psi_i | \Psi_l \rangle} - \frac{\sum_{i,l} \mathcal{H}_{il} c_{ji}^* c_{jl} \sum_l \mathcal{S}_{ml} c_{jl}}{\left(\sum_{i,l} \mathcal{S}_{il} c_{ji}^* c_{jl} \right)^2} = 0 \quad (1.9)$$

The minimum values of the eigenvalues ϵ_j are found when optimized with respect to c_{ij}^* , obtaining Equation (1.9). The optimization leads to the matrix equation

$$\sum_l \mathcal{H}_{ml} c_{jl} = \epsilon_j \sum_l \mathcal{S}_{ml} c_{jl}, \quad (1.10)$$

which may be expressed in matrix form as $\mathcal{H}\boldsymbol{\psi}_j = \epsilon_j \mathcal{S}\boldsymbol{\psi}_j$, where each column vector is defined as $\boldsymbol{\psi}_j = (c_{j1}, c_{j2}, \dots, c_{jN})$ over all n wavefunctions in the unit cell. The overlap matrix \mathcal{S} quantifies the physical overlap between atomic orbitals located on adjacent atoms within the lattice, and therefore contributes to the eigenvalues

ϵ_j . These are finally found by solving the secular equation

$$\det(\mathcal{H} - \epsilon_j \mathcal{S}) = 0, \quad (1.11)$$

returning n eigenvalues for a given $\boldsymbol{\kappa}$ at symmetrical points in the unit cell.

In graphene, the matrix indices obey the sublattice structure in Equation (1.4), therefore $i = \lambda$ and $j = \lambda'$, for two atomic orbitals for π electrons. The elements of the Hamiltonian matrix (1.12) are commonly referred to as the transfer integrals. These elements characterize the hopping of electrons between atomic sites and change depending on the interacting sublattices. The elements of \mathcal{S} , often referred to as overlap integrals, are illustrated by Equation (1.13).

$$\mathcal{H}_{\lambda\lambda'} = \frac{1}{N} \sum_{\mathbf{R}_\lambda, \mathbf{R}_{\lambda'}} e^{i\boldsymbol{\kappa} \cdot (\mathbf{R}_{\lambda'} - \mathbf{R}_\lambda)} \langle \phi_\lambda(\mathbf{r} - \mathbf{R}_\lambda) | \mathcal{H} | \phi_{\lambda'}(\mathbf{r} - \mathbf{R}_{\lambda'}) \rangle \quad (1.12)$$

$$\mathcal{S}_{\lambda\lambda'} = \frac{1}{N} \sum_{\mathbf{R}_\lambda, \mathbf{R}_{\lambda'}} e^{i\boldsymbol{\kappa} \cdot (\mathbf{R}_{\lambda'} - \mathbf{R}_\lambda)} \langle \phi_\lambda(\mathbf{r} - \mathbf{R}_\lambda) | \phi_{\lambda'}(\mathbf{r} - \mathbf{R}_{\lambda'}) \rangle \quad (1.13)$$

It is noteworthy that the complex phase factor in the summation (1.12) represents the displacement between atom sites to a defined neighbor number m , $\mathbf{R}_{\lambda'} - \mathbf{R}_\lambda = \boldsymbol{\tau}_m^{(j)}$, which represents the neighboring sites under consideration. The integral contains a matrix element of the Hamiltonian in the $|\phi_\lambda\rangle$ basis. This has

been redefined as the hopping terms (1.14).

$$t_m \equiv \langle \phi_\lambda(\mathbf{r} - \mathbf{R}_\lambda) | \hat{\mathcal{H}} | \phi_{\lambda'}(\mathbf{r} - \mathbf{R}_\lambda - \boldsymbol{\tau}_m^{(j)}) \rangle \quad (1.14)$$

$$s_m \equiv \langle \phi_\lambda(\mathbf{r} - \mathbf{R}_\lambda) | \phi_{\lambda'}(\mathbf{r} - \mathbf{R}_\lambda - \boldsymbol{\tau}_m^{(j)}) \rangle \quad (1.15)$$

The Slater-Koster scheme neglects overlap integrals, i.e., $\mathcal{S}_{\lambda\lambda'} = 0$ for any $\lambda \neq \lambda'$, and only on-site overlaps are $\mathcal{S}_{AA} = 1$, enabling the approximation $\mathcal{S} = \mathbf{1}^9$. However, the complete scheme considers the overlap scalars $s_{AA'}$ (1.15) for as many neighbors as needed. In this case, we have s_1 , s_2 , and s_3 for the first, second, and third neighbors, respectively. These are real numbers. Many calculations conducted in this study will employ the Slater-Koster scheme to simplify the problem. Consequently, in graphene, the off-diagonal elements of the overlap matrix \mathcal{S} are set to zero ($\mathcal{S}_{AB} = \mathcal{S}_{BA} = 0$), unless otherwise specified.

1.2 Transfer and Overlap Integrals

1.2.1 Hamiltonian and overlap matrix elements

In the context of the three nearest-neighbors approximation, the diagonal elements of the Hamiltonian consider both the on-site energy $\tilde{\epsilon}_{2p}$ and the t_2 hopping term between the same lattice. Conversely, the off-diagonal elements contain the t_1 and

t_3 hopping terms between different lattices. These parameters are real scalars.

$$\mathcal{H}_{AA} = \mathcal{H}_{AA}^{(0)} + \mathcal{H}_{AA}^{(2)} = \tilde{\epsilon}_{2p} + t_2 f_2(\boldsymbol{\kappa}) \quad (1.16)$$

$$\mathcal{H}_{AB} = \mathcal{H}_{AB}^{(1)} + \mathcal{H}_{AB}^{(3)} = t_1 f_1(\boldsymbol{\kappa}) + t_3 f_3(\boldsymbol{\kappa}) \quad (1.17)$$

The diagonal terms (1.16) are equivalent across sub-lattices, i.e. ($\mathcal{H}_{AA} = \mathcal{H}_{BB}$), as both contain identical carbon atoms. Additionally, the off-diagonal elements (1.17) are each other's complex conjugates ($\mathcal{H}_{BA} = \mathcal{H}_{AB}^*$).

Notice the super-indices represent the neighbor number. Also, the appearance of the terms $f_i(\boldsymbol{\kappa})$, which re-scale and add a phase shift to the hopping terms, depends on the neighbor number ($i = 0, 1, 2, 3$). As an example, let's calculate the on-site energy $i = 0$. The summation occurs so that every neighboring orbital is itself, i.e. the distance between neighbors is $\mathbf{R}'_A - \mathbf{R}_A = \mathbf{0}$.

$$\mathcal{H}_{AA} = \frac{1}{N} \sum_{\mathbf{R}'_A = \mathbf{R}_A} e^{i\boldsymbol{\kappa} \cdot (\mathbf{R}'_A - \mathbf{R}_A)} \langle \phi_A(\mathbf{r} - \mathbf{R}_A) | \hat{\mathcal{H}} | \phi_A(\mathbf{r} - \mathbf{R}'_A) \rangle \quad (1.18)$$

$$\mathcal{H}_{AA} = \frac{1}{N} \sum_{\mathbf{R}'_A = \mathbf{R}_A} e^{i\boldsymbol{\kappa} \cdot \mathbf{0}} \tilde{\epsilon}_{2p} \langle \phi_A(\mathbf{r} - \mathbf{R}_A) | \phi_A(\mathbf{r} - \mathbf{R}_A) \rangle \quad (1.19)$$

The basis for the p_z orbitals is orthonormal, so the term $\langle \phi_A | \phi_A \rangle = 1$. The phase shift in this case is zero, and no dependence on $\boldsymbol{\kappa}$ is left. The summation then spans all sites in the lattice, as shown in (1.20).

$$\mathcal{H}_{AA}^{(0)} = \frac{1}{N} \sum_{i=1}^N \tilde{\epsilon}_{2p} = \tilde{\epsilon}_{2p} \quad (1.20)$$

The case for $\mathcal{H}_{AA}^{(2)}$ is slightly different, since a phase is induced by the hopping of electrons between neighboring sites. The geometry that satisfies this criterion is $\mathbf{R}'_A - \mathbf{R}_A = \boldsymbol{\tau}_2^{(j)}$. As shown in Equation (1.6) and Figure 1.2b, there are $j = 1, \dots, 6$ second nearest-neighbors that belong to the same lattice.

$$\mathcal{H}_{AA}^{(2)} = \frac{1}{N} \sum_{\mathbf{R}'_A = \mathbf{R}_A + \boldsymbol{\tau}_2^{(j)}} e^{i\boldsymbol{\kappa} \cdot (\mathbf{R}'_A - \mathbf{R}_A)} \langle \phi_A(\mathbf{r} - \mathbf{R}_A) | \hat{\mathcal{H}} | \phi_A(\mathbf{r} - \mathbf{R}'_A) \rangle, \quad (1.21)$$

$$\mathcal{H}_{AA}^{(2)} = t_2 f_2(\boldsymbol{\kappa}), \quad \text{where} \quad f_2(\boldsymbol{\kappa}) \equiv \sum_{j=1}^6 e^{i\boldsymbol{\kappa} \cdot \boldsymbol{\tau}_2^{(j)}}. \quad (1.22)$$

The resulting energy term (1.22) is the product of a hopping term t_2 , and the second nearest-neighbor phase factor f_2 . The remaining transfer integrals are computed in a similar manner.

$$\mathcal{H}_{AB}^{(1)} = t_1 f_1(\boldsymbol{\kappa}), \quad f_1(\boldsymbol{\kappa}) \equiv \sum_{j=1}^3 e^{i\boldsymbol{\kappa} \cdot \boldsymbol{\tau}_1^{(j)}} \quad (1.23)$$

$$\mathcal{H}_{AB}^{(3)} = t_3 f_3(\boldsymbol{\kappa}), \quad f_3(\boldsymbol{\kappa}) \equiv \sum_{j=1}^3 e^{i\boldsymbol{\kappa} \cdot \boldsymbol{\tau}_3^{(j)}} \quad (1.24)$$

The overlap matrix elements (1.25) and (1.26) each contain an overlap term associated with a nearest-neighbor. These are listed in (1.27).

$$\mathcal{S}_{AA} = \mathcal{S}_{AA}^{(0)} + \mathcal{S}_{AA}^{(2)} = 1 + s_2 f_2(\boldsymbol{\kappa}) \quad (1.25)$$

$$\mathcal{S}_{AB} = \mathcal{S}_{AB}^{(1)} + \mathcal{S}_{AB}^{(3)} = s_1 f_1(\boldsymbol{\kappa}) + s_3 f_3(\boldsymbol{\kappa}) \quad (1.26)$$

When comparing the definition of the overlap (1.13) and transfer integrals

(1.12), the most notable difference is the Hamiltonian operator $\hat{\mathcal{H}}$. It re-centers the orbital functions $\phi_\lambda(\mathbf{r} - \mathbf{R}_\lambda)$, simplifying the inner product term. In the case of the overlap integrals, there is no operator, so the inner products are not obvious. However, these have the same value for all sites which belong to the same neighbor number. For instance, all overlaps s_1 are the same for all $j = 1, \dots, 3$.

$$\begin{aligned} s_1 &= \langle \phi_A(\mathbf{r} - \mathbf{R}_A) | \phi_B(\mathbf{r} - \mathbf{R}_B - \boldsymbol{\tau}_1^{(j)}) \rangle, \quad \forall j = 1, \dots, 3 \\ s_2 &= \langle \phi_A(\mathbf{r} - \mathbf{R}_A) | \phi_A(\mathbf{r} - \mathbf{R}_A - \boldsymbol{\tau}_2^{(j)}) \rangle, \quad \forall j = 1, \dots, 6 \\ s_3 &= \langle \phi_A(\mathbf{r} - \mathbf{R}_A) | \phi_B(\mathbf{r} - \mathbf{R}_B - \boldsymbol{\tau}_3^{(j)}) \rangle, \quad \forall j = 1, \dots, 3 \end{aligned} \quad (1.27)$$

1.2.2 Phase factors

All phase factors are sums of exponential functions that can be manipulated into more comprehensible equations. The first (1.28) and third (1.29) phase factors are very similar, since $|\boldsymbol{\tau}_3| = 2|\boldsymbol{\tau}_1|$. Both are complex valued functions:

$$f_1(\boldsymbol{\kappa}) = \left(e^{i\frac{a\kappa_x}{2}} + e^{-i\frac{a\kappa_x}{2}} \right) e^{-i\frac{a\kappa_y}{2\sqrt{3}}} + e^{i\frac{a\kappa_y}{\sqrt{3}}} = e^{i\frac{a\kappa_y}{\sqrt{3}}} + 2e^{-i\frac{a\kappa_y}{2\sqrt{3}}} \cos\left(\frac{a\kappa_x}{2}\right), \quad (1.28)$$

$$f_3(\boldsymbol{\kappa}) = \left(e^{i\kappa_x a} + e^{-i\kappa_x a} \right) e^{i\frac{\kappa_y a}{\sqrt{3}}} + e^{-i\frac{2\kappa_y a}{\sqrt{3}}} = e^{-\frac{2i\kappa_y a}{\sqrt{3}}} + 2e^{\frac{i\kappa_y a}{\sqrt{3}}} \cos(\kappa_x a). \quad (1.29)$$

The second nearest-neighbor phase factor (1.30) is a real valued function, so it

re-scales the hopping and overlap terms, as a function of κ as shown:

$$\begin{aligned} f_2(\boldsymbol{\kappa}) &= \left(e^{i\frac{a}{2}\kappa_x} + e^{-i\frac{a}{2}\kappa_x} \right) \left(e^{i\frac{\sqrt{3}}{2}a\kappa_y} + e^{-i\frac{\sqrt{3}}{2}a\kappa_y} \right) + 2 \cos(a\kappa_x), \\ f_2(\boldsymbol{\kappa}) &= 4 \cos\left(\frac{\sqrt{3}a\kappa_y}{2}\right) \cos\left(\frac{a\kappa_x}{2}\right) + 4 \cos^2\left(\frac{a\kappa_x}{2}\right) - 2. \end{aligned} \quad (1.30)$$

There is a relation between f_1 and f_2 that helps simplify analytical manipulations when solving for the eigenvalues of the Hamiltonian matrix. The simplest identity is obtained by calculating the squared absolute value of f_1 is (1.32), and comparing it to (1.30). From now on, we redefine $f(\boldsymbol{\kappa}) \equiv f_1(\boldsymbol{\kappa})$.

$$|f(\boldsymbol{\kappa})|^2 = f_1^* f_1 = 4 \cos\left(\frac{\sqrt{3}\kappa_y a}{2}\right) \cos\left(\frac{\kappa_x a}{2}\right) + 4 \cos^2\left(\frac{\kappa_x a}{2}\right) + 1 \quad (1.31)$$

$$f_2(\boldsymbol{\kappa}) = |f(\boldsymbol{\kappa})|^2 - 3 \quad (1.32)$$

1.3 Eigenvalue equation

The eigenvalue equation at \mathbf{K} yields a characteristic polynomial $P(\epsilon)$ with two possible eigenvalues ϵ_+ and ϵ_- , and eigenvectors $\boldsymbol{\psi}_+$ and $\boldsymbol{\psi}_-$. Using matrix elements (1.16), (1.17), (1.25), and (1.26), the $P(\epsilon)$ polynomial takes the form

$$P(\epsilon) = \det(\mathcal{H} - \epsilon\mathcal{S}) = (\mathcal{H}_{AA} - \epsilon\mathcal{S}_{AA})^2 - |\mathcal{H}_{AB} - \epsilon\mathcal{S}_{AB}|^2 = 0. \quad (1.33)$$

Notice the absolute value makes it difficult to solve for ϵ in some cases. The

relation (1.32) allows for a convenient redefinition of the on-site energy, as shown in (1.34). Consequently, the matrix element \mathcal{H}_{AA} changes according to (1.35), and the \mathcal{S}_{AA} term changes similarly. The eigenvalues are then obtained by cases.

$$\tilde{\epsilon}_{2p} = \epsilon_{2p} - 3t_2 \quad (1.34)$$

$$\mathcal{H}_{AA} = \epsilon_{2p} + t_2 |f(\boldsymbol{\kappa})|^2 \quad (1.35)$$

These relations also allow us to express the Hamiltonian matrix in a more condensed form (1.36). Since this is a 2×2 matrix, the eigenvalue equation will yield a characteristic polynomial $P(\epsilon)$ with two possible eigenvalues ϵ_+ and ϵ_- , and corresponding eigenvectors $\boldsymbol{\psi}_+$ and $\boldsymbol{\psi}_-$. This matrix can be manipulated to find simpler approximations for graphene, if needed.

$$\mathcal{H} = \begin{pmatrix} \epsilon_{2p} + t_2 |f(\boldsymbol{\kappa})|^2 & t_1 f(\boldsymbol{\kappa}) + t_3 f_3(\boldsymbol{\kappa}) \\ t_1 f^*(\boldsymbol{\kappa}) + t_3 f_3^*(\boldsymbol{\kappa}) & \epsilon_{2p} + t_2 |f(\boldsymbol{\kappa})|^2 \end{pmatrix} \quad (1.36)$$

After solving the characteristic equation for the nearest neighbors Hamiltonian and rearrangement of terms, and introducing the variable $n = \pm 1$, which defines the two energy bands of the π electrons, we have the eigenvalue

$$\epsilon_n(\boldsymbol{\kappa}) = \frac{\epsilon_{2p} + nt_1 |f(\boldsymbol{\kappa})|}{1 + ns_1 |f(\boldsymbol{\kappa})|}. \quad (1.37)$$

The first-nearest neighbors approximation takes $t_2 = t_3 = 0$ and $s_2 = s_3 = 0$. The terms $t_1 = -3.070$ eV, $s_1 = 0.070$ eV^{6,10} differ by two orders of magnitude,

which suggests that overlap integrals might be negligible in systems like graphene in particular situations. The energy eigenvalues for the next-nearest neighbors Hamiltonian are obtained by solving the characteristic polynomial, and using a similar rearrangement of terms as before, obtaining (1.38).

$$\epsilon_n(\boldsymbol{\kappa}) = \frac{\epsilon_{2p} + nt_1|f(\boldsymbol{\kappa})| + t_2|f(\boldsymbol{\kappa})|^2}{1 + ns_1|f(\boldsymbol{\kappa})| + s_2(3 + |f(\boldsymbol{\kappa})|^2)} \quad (1.38)$$

The eigenvectors $\boldsymbol{\psi}_+$ and $\boldsymbol{\psi}_-$ (1.39) are obtained by replacing each ϵ_+ and ϵ_- back into $\mathcal{H} - \epsilon_n \mathbb{1} = \mathbf{0}$, and then row reducing the matrix. Let's define the function $\hat{f}(\boldsymbol{\kappa}) = f/|f|$. The property $f - f^* = 0$ holds. The complete process of row reduction is shown in Annex B.

$$\boldsymbol{\psi}_+ = \frac{1}{\sqrt{2}} \begin{pmatrix} 1 \\ \hat{f}^* \end{pmatrix}, \quad \boldsymbol{\psi}_- = \frac{1}{\sqrt{2}} \begin{pmatrix} -\hat{f} \\ 1 \end{pmatrix}. \quad (1.39)$$

The matrix $\mathcal{H} - \epsilon\mathcal{S}$ for the next next-nearest neighbors takes the complete form (1.36). The analytic expression for the eigenvalues in this case is complicated since there is no explicit relation between the variables s_1 , s_3 , f and f_3 . Therefore, the three-neighbor approximation will be only addressed using a Taylor expansion of the phase factors f and f_3 .

A series expansion of the elements of the Hamiltonian around high symmetry points \mathbf{K} contains several material-dependent coefficients, which are shown in complete form in Annex C. Notice that the Hamiltonian satisfies $\mathcal{H}_{AB} = \mathcal{H}_{BA}^*$ and $\mathcal{H}_{AB} = \mathcal{H}_{BA}^*$ to be a Hermitian operator.

1.4 Spin-Orbit Coupling Hamiltonian

The physics of interest in this system occurs around the Fermi level, which is located at 0, where both valence and conduction bands for the π electrons touch, at the high symmetry points $\pm\mathbf{K}$, as shown in Figure 1.3a.

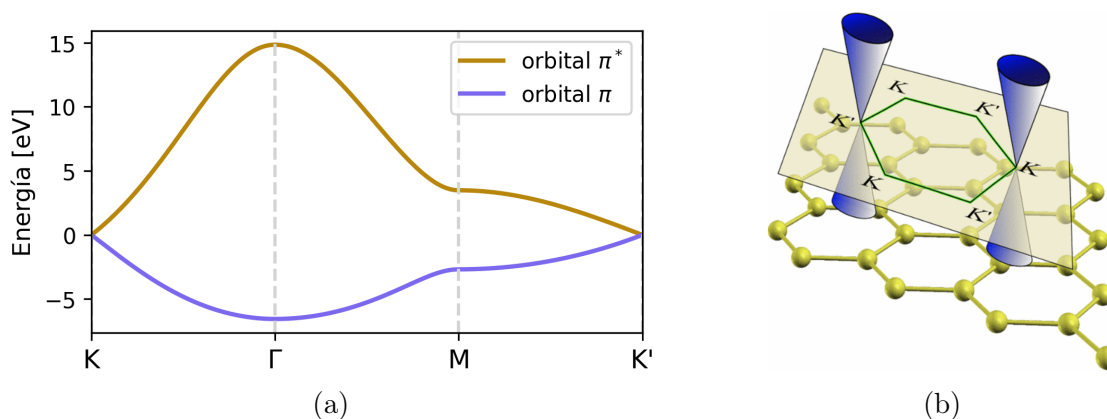


Figure 1.3: (a) Bands at points of high symmetry at the edge of the first Brillouin zone. (b) Energy surfaces around Dirac points².

Pristine graphene is famous for having a dispersion relation dominated by k -linear terms around the high symmetry points $\pm\mathbf{K}$, where k is the magnitude of the momentum vector. These are often called the Dirac points, because the energy surfaces of π electrons in the vicinity of these points, which are shown in Figure 1.3b, resemble those for the massless free fermions from the Dirac equation³.

The interesting fact is that after adding perturbations to the system, this symmetry breaks and the apparent relativistic behavior in graphene disappears. The first perturbation to consider is the intrinsic spin-orbit coupling (SOC) in graphene, which induces spectral gaps at the Dirac points, right on top of the smallest gap

between the conduction and valence bands. This effect is seen from second-nearest neighbors onwards. SOC could have important applications in quantum computing due to its relatively long spin lifetimes, enough for us to use electron spins as carriers of information⁴, as well as a long mean free path which is useful for spintronics¹¹. The Hamiltonian for this system is³

$$\mathcal{H}_{\text{so}}(\boldsymbol{\kappa}) = \begin{pmatrix} h_{\text{so}} & 0 \\ 0 & -h_{\text{so}} \end{pmatrix} = \sigma_z \otimes h_{\text{so}} \equiv \sigma_z h_{\text{so}}, \quad (1.40)$$

where h_{so} is a 2×2 matrix by definition (1.41). Notice the SOC hopping constant value is $\lambda_{\text{so}} = 12\mu\text{eV}^4$, which is significantly smaller than the hopping and overlap terms for the first-nearest neighbors approximation.

$$h_{\text{so}} = i\lambda_{\text{so}} \sum_{j,k} \mathbf{s} \cdot (\boldsymbol{\tau}_1^{(j)} \times \boldsymbol{\tau}_1^{(k)}) e^{i\boldsymbol{\kappa} \cdot (\boldsymbol{\tau}_1^{(j)} - \boldsymbol{\tau}_1^{(k)})} \quad (1.41)$$

It is evident that since the first-nearest neighbor vectors exist in the xy plane, the cross product $\boldsymbol{\tau}_1^{(j)} \times \boldsymbol{\tau}_1^{(k)}$ only contains elements in the z direction. As a consequence, the only spin matrix element involved is s_z . This simplifies the calculation of the complete analytic term as shown:

$$h_{\text{so}} = \frac{2\sqrt{3}a^2s_z}{3} \sin\left(\frac{\kappa_x a}{2}\right) \left[\cos\left(\frac{\sqrt{3}\kappa_y a}{2}\right) - \cos\left(\frac{\kappa_x a}{2}\right) \right]. \quad (1.42)$$

When h_{so} is expanded in series as shown in Equation (1.43), the intrinsic SOC term is evident as the first term independent of \mathbf{k} . The SOC Hamiltonian then

can be written in its most simple form as (1.44).

$$h_{\text{so}} = a^2 s_z \left(\frac{3}{2} - \frac{3}{8} a^2 [k_x^2 + k_y^2] + \dots \right) \quad (1.43)$$

$$\mathcal{H}_{\text{so}}(\boldsymbol{\kappa}) = \frac{3}{2} \lambda_{\text{so}} a^2 s_z + \mathcal{O}(a^2 \mathbf{k}^2) \quad (1.44)$$

The final expression of the Hamiltonian using the TB model is of the form (1.45). Notice it is a function of the Pauli matrices σ_j , up to third order on the wave vector components, which were recognized from equations (5.1) and only the first term of the expansion (1.44).

$$\begin{aligned} \mathcal{H}(\mathbf{k}) = & \epsilon_{2p} \mathbb{1} + \frac{3}{4} a^2 t_2 \mathbb{1} (k_x^2 + k_y^2) + \frac{\sqrt{3}}{8} a^3 t_2 \mathbb{1} k_x [-k_x^2 + 3k_y^2] + \frac{3}{2} \lambda_{\text{so}} a^2 s_z \\ & + a \left(-\frac{\sqrt{3}t_1}{2} + \sqrt{3}t_3 \right) [\sigma_x k_x + \sigma_y k_y] \\ & - a^2 \left(\frac{t_1}{8} + \frac{t_3}{2} \right) [\sigma_x (-k_x^2 + k_y^2) + \sigma_y 2k_x k_y] \\ & + a^3 \left(\frac{\sqrt{3}t_1}{48} - \frac{\sqrt{3}t_3}{6} \right) [\sigma_x k_x (k_x^2 + k_y^2) + \sigma_y k_y (k_x^2 + k_y^2)] \end{aligned} \quad (1.45)$$

1.5 Adding new physics systematically

It is possible to keep adding terms to the Hamiltonian by considering more physical fields and new perturbation Hamiltonians. One example is the SOC Hamiltonian

$\mathcal{H}_R(\boldsymbol{\kappa})$ under an external electric \mathcal{E} field, which is defined as:

$$\mathcal{H}_R(\boldsymbol{\kappa}) = \begin{pmatrix} 0 & h_R \\ h_R^* & 0 \end{pmatrix}, \quad \text{where} \quad h_R = \lambda_R \mathbf{S} \cdot \boldsymbol{\mathcal{E}} \times \sum_j i\boldsymbol{\tau}_1^{(j)} e^{i\boldsymbol{\kappa} \cdot \boldsymbol{\tau}_1^{(j)}}. \quad (1.46)$$

The drawback with this approach is the lack of a systematic method and criteria to add relevant physical terms to the systems. Usually, after expanding Hamiltonian (1.46), Rashba spin-orbit coupling type of contributions are often ignored³. In systems with low molecular weight atoms like carbon, this is no problem, but in larger systems, ignoring these kinds of terms might result in an incomplete model.

One solution is to use group theory methods to consider all possible operators that describe a molecular lattice according to its symmetries. The work of Bir & Pikus¹² on invariant expansion allows the construction of Hamiltonians using basis functions that obey the symmetry operations that leave the crystal invariant. This approach exploits the symmetries of the lattice and introduces criteria to describe the physics, without having to guess or do long and error-prone approximations.

Chapter 2

Methods

The procedure to generate a Hamiltonian for graphene's π electrons consists of five steps. First, the molecule has to be analyzed to identify its point group \mathcal{G} . In this case, it is necessary to only consider the geometry of the sublattices A and B. Second, a proper basis set needs to be used to diagonalize the Hamiltonian. This basis transforms according to an irreducible representation Γ_κ of \mathcal{G} . Third, a reducible representation that describes the Hamiltonian is chosen and then reduced. Fourth, the physics that describes the system is identified to pick appropriate basis functions that describe the system. It is valid to pick different physical fields or tensor operators like momentum \mathbf{k} , electric field \mathcal{E} , magnetic field \mathcal{B} , spin vector operator \mathbf{s} , strain tensor ϵ_{ij} , and many more. Lastly, the Hamiltonian is expanded as a series of basis functions and physical constants to the desired order. The main concepts will be explained thoroughly, and many examples will be introduced.

2.1 Principles of theory of invariants

The symmetry of a crystal is characterized by a set of transformations that leave it invariant; that is, with every site of the crystal unchanged. This set and its operations are called a group^{9,12}. Formally, a group is a set \mathcal{G} together with a binary operation $\mathcal{G} \times \mathcal{G} \rightarrow \mathcal{G}$, which satisfy four properties:

1. **Closure:** For all $a, b \in \mathcal{G}$ the product ab is also in \mathcal{G} .
2. **Associativity:** For all $a, b, c \in \mathcal{G}$, the equation $(ab)c = a(bc)$ holds.
3. **Identity element:** There exists $e \in \mathcal{G}$ such that $ea = ae \forall a \in \mathcal{G}$.
4. **Inverse element:** There exists $a^{-1} \in \mathcal{G}$ such that $a^{-1}a = aa^{-1} = e \forall a \in \mathcal{G}$.

An element $g \in \mathcal{G}$ is called a symmetry operation. There are many spatial groups of interest in condensed matter physics; however, the one of our concern is called a point group, which is the group of all rotations R , proper or improper, that leave the crystal invariant. A proper rotation is a simple rotation about a coordinate axis. An improper rotation, or roto-reflection, is a rotation plus a reflection in a plane perpendicular to the rotation axis^{9,12}.

Initially, symmetry operations g of a point group are abstract objects, which need a particular form to be used. Let ψ_ν be a set of n single-valued linearly independent functions of a point $\mathbf{x}(x_1, x_2, x_3)$ in the xyz coordinate system. Let $\mathbf{x}(x'_1, x'_2, x'_3)$ be the same point, in the new coordinate system $x'y'z'$, which is

obtained from xyz by the transformation g . The coordinates of $\mathbf{x}(x', y', z')$ in the new system are the coordinates of the vector $g^{-1}\mathbf{x}$ in the initial system:

$$x'_\nu = (g^{-1}\mathbf{x})_\nu = \sum_{\mu} \mathcal{R}_{\nu\mu}(g^{-1})x_\mu = \sum_{\mu} \mathcal{R}_{\mu\nu}(g)x_\mu, \quad (2.1)$$

since the same rotation of both the coordinate system and the vector leaves its coordinates unchanged¹². Now, let $\mathcal{D}(g) : \psi_\nu \rightarrow \psi_s$, such that:

$$\mathcal{D}(g)\psi_\nu(\mathbf{x}) = \psi_\nu(g^{-1}\mathbf{x}) = \sum_{\mu} \mathcal{D}_{\mu\nu}(g)\psi_\mu(g\mathbf{x}) = \psi_s(\mathbf{x}) \quad (2.2)$$

Notice that both operators $\mathcal{R}(g)$ and $\mathcal{D}(g)$ are different, because they act on different sets of vectors. The only case where $\mathcal{R}(g) = \mathcal{D}(g)$ holds, is when $\psi_\nu = x_\nu \forall \nu = 1, 2, \dots, n$. Generally, $\mathcal{R}(g) \neq \mathcal{D}(g)$ ¹². Anyways, the set of all $\mathcal{D}(g) \forall g \in \mathcal{G}$ is called a representation Γ . The form of $\mathcal{D}(g)$ will depend on the choice of the ψ_ν functions. Matrices $\mathcal{R}(g)$ also form a representation, which describes rotations of space, and not of functions of space.

There are several properties of representations Γ that are of interest. The dimensionality m of a representation is equal to the dimension of each of its matrices. Importantly, these are not unique, since there is always a unitary similarity (or equivalence) transformation U which generates a new set of matrices by the product $U\mathcal{D}(g)U^{-1}$, which form a valid representation⁹.

These can also be combined as block matrices to form new representations. Let $g \in \mathcal{G}$ have two representations Γ and Γ' , each being in matrix form: ℓ -dimensional

$\mathcal{D}(g)$ and ℓ' -dimensional $\mathcal{D}'(g)$, respectively. The new combined representation Γ'' has the block form for all $g \in \mathcal{G}$:

$$\Gamma'' = \Gamma \oplus \Gamma' \quad \Longrightarrow \quad \mathcal{D}''(g) = \begin{pmatrix} \mathcal{D}(g) & \mathcal{O} \\ \mathcal{O} & \mathcal{D}'(g) \end{pmatrix}, \quad (2.3)$$

where \mathcal{O} is an $\ell \times \ell'$ dimensional null matrix. It can be concluded that Γ'' representation is $\ell + \ell'$ dimensional.

An important property of Γ'' is that it is a reducible representation, because $\mathcal{D}''(g)$ has the same block form for all elements in the group. If $\mathcal{D}''(g)$ was not in block form, then there exists a unitary similarity transformation U that operates such that $\Gamma'' : U\mathcal{D}''(g)U^{-1}$ is in block form. If by the contrary, a representation $\Gamma'' : \mathcal{D}''(g)$ is such that no similarity transformation makes all matrices in Γ'' acquire the same block form, then Γ'' is an irreducible representation; irrep, for short. Now, consider that representations Γ and Γ' are irreps, then the direct sum in Equation (2.3) is known as the reduction of Γ'' into its irreducible constituents.

Finally, an important aspect of the theory of invariants is invariance. A Hamiltonian \mathcal{H} is invariant under a transformation g in the group \mathcal{G} , such that it satisfies the condition (2.4)¹². Notice the transformation happens on the tensor \mathcal{K} , and also on the matrix \mathcal{H} , using the matrix representation $\mathcal{D}(g)$.

$$\mathcal{H}'(\mathcal{K}') = \mathcal{D}(g)\mathcal{H}(g^{-1}\mathcal{K})\mathcal{D}^{-1}(g) = \mathcal{H}(\mathcal{K}), \quad \forall g \in \mathcal{G}. \quad (2.4)$$

2.2 Symmetry operations in D_{3h}

The honeycomb lattice in Figure 1.1a shows that each atom in a sublattice A or B satisfies the symmetry operations of a D_{3h} point group. This group is characterized by six ($k = 1, \dots, 6$) classes of rotations: one identity operation E , one horizontal reflection σ_h , two in-plane 120° rotation $2C_3$ about the principal axis, two in-plane 120° improper rotations $2S_3$, three vertical mirror plane rotation 90° rotations $3C'_2$, and three vertical reflections $3\sigma_v$. For consistency, atoms on each sub-lattice are named according to Figure 2.1⁴.

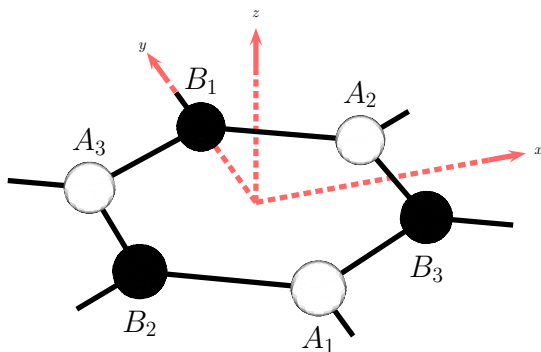


Figure 2.1: Standard axis and atom labeling convention for pristine graphene.

The rotation axes and planes of reflection are shown in Figure 2.2. The in-plane rotation C_3 happens around the orientation \mathbf{z} , which comes out of the plane, as shown in Figure 2.1. The improper rotations S_3 are C_3 rotations followed by the vertical reflection σ_h , inverting the perpendicular direction $-\mathbf{z}$.

There are six classes in D_{3h} , and there is one matrix for each element in the class. Annex D contains every matrix representation of symmetry elements in D_{3h} generated using vector $\boldsymbol{\kappa}$, according to the reference frame in Figure 1.1b. All

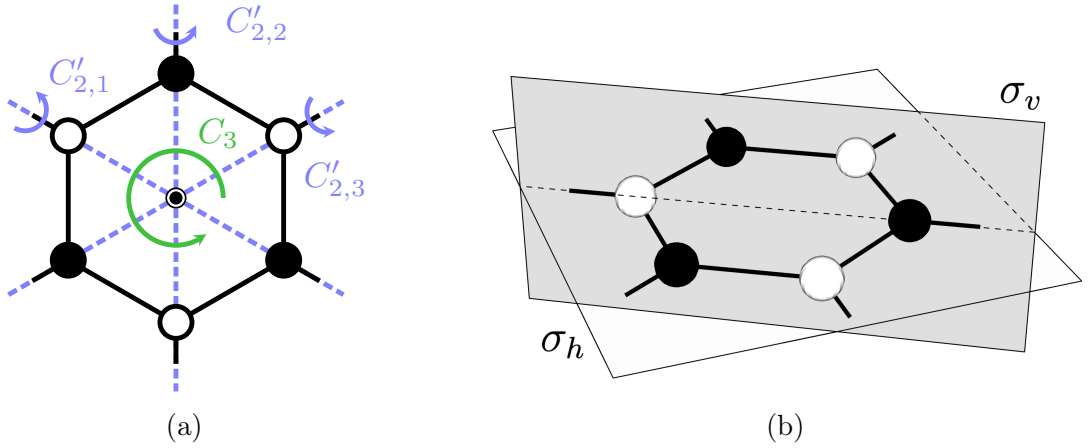


Figure 2.2: Symmetry operations of graphene sub-lattices: (a) axes of proper rotation, and (b) planes of reflection. The shaded plane is one of the three vertical reflection planes σ_v , while the graphene plane is the horizontal reflection σ_h .

operations on the honeycomb lattice are shown in Figure 2.3.

2.3 Symmetry elements acting on the operator \mathcal{K}

Applying a symmetry operation g from the group D_{3h} to the tensor operator \mathcal{K} , we transform it as $\mathcal{K} \rightarrow g\mathcal{K}$. This allows us to reexpress the Hamiltonian \mathcal{H}' in new coordinates. Consider a Hamiltonian like (1.45), which depends entirely on the components of the momentum vector. To transform these components, we use the matrix representation of the symmetry element, denoted by $R(g)$. The transformation of the momentum vector is given by $\mathbf{k}' = R(g)\mathbf{k}$. Consequently, the tensor elements after this transformation are given by the equation:

$$g\mathcal{K}_l^{(\kappa,\lambda)} = f(\mathbf{k}') = f(k'_x, k'_y, k'_z). \quad (2.5)$$

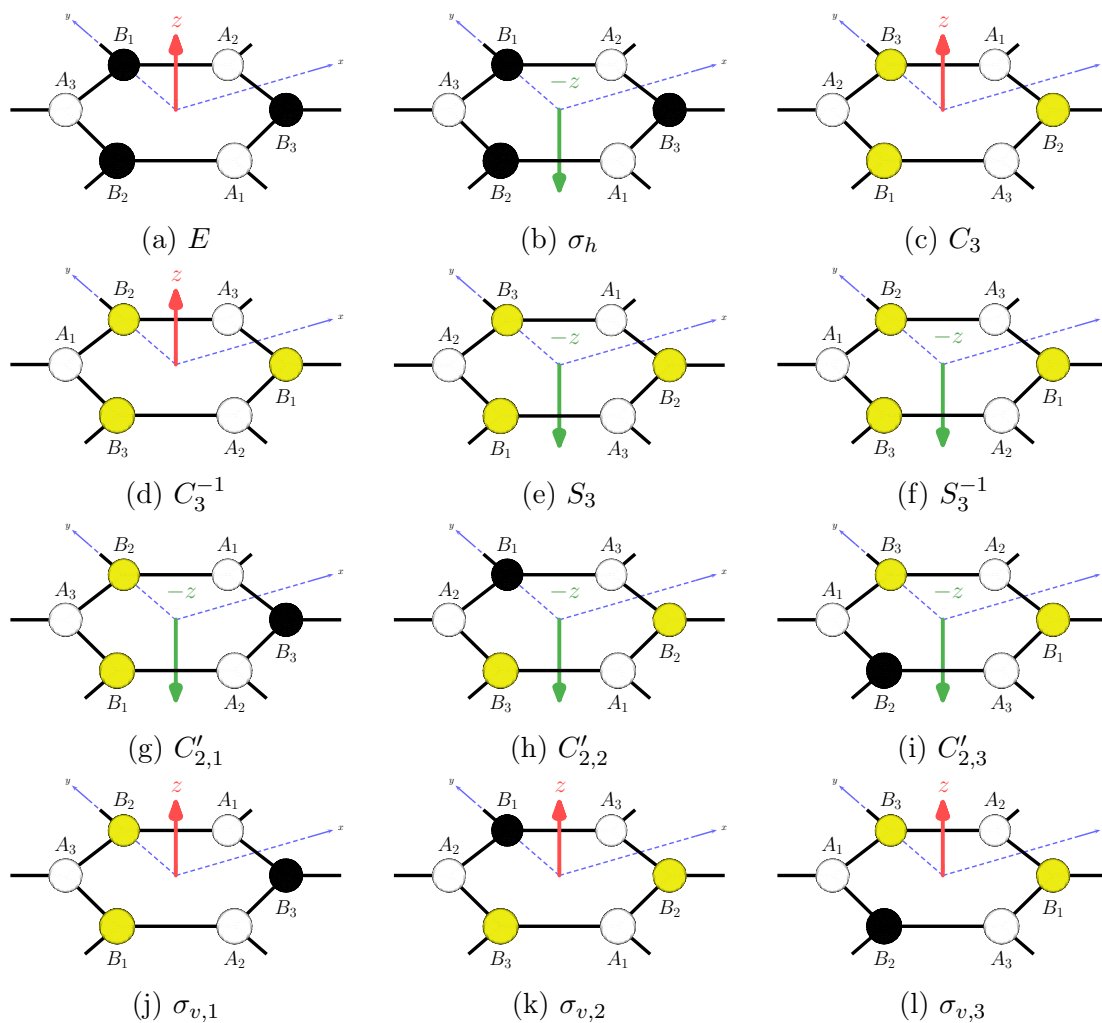


Figure 2.3: D_{3h} symmetry operations on graphene. The figures show atoms in the B sublattice switching positions with respect to the identity element E . The vector \mathbf{z} is green when the operation switches the direction of the plane. The original system of reference in blue is left for reference.

Lets take as an example the basis functions for the irrep Γ_6 of the invariant expansion for the block Hamiltonian in the right Dirac point (3.3). The tensor components for this irrep are closed under transformations $\mathcal{R}^{(\Gamma_6)}(g)$ for all $g \in D_{3h}$ ⁹. This means two things in group theory. First, there exists a partner set β_n which contains elements of the tensor operator of n -th order. Second, each

transformed tensor element $g\mathcal{K}_l^{(\kappa,\lambda)}$ is a linear combination of the elements in β_n . The union of all the partner sets form the basis functions for the irrep Γ_6 .

Lets define $M \equiv \mathcal{R}^{(\Gamma_6)}(C_3)$ as the matrix representation of C_3 for this irrep. According to the invariance equation (2.4), first we need to transform the tensor using g^{-1} . Each transformed element is of the form $k'_i = M_{ij}^{-1}k_j$, and for the two components k_x and k_y associated with Γ_6 on the graphene plane we have

$$\begin{aligned} C_3^{-1} k_x &\equiv k'_x = M_{11}^{-1}k_x + M_{12}^{-1}k_y = -\frac{1}{2}k_x + \frac{\sqrt{3}}{2}k_y, \\ C_3^{-1} k_y &\equiv k'_y = M_{21}^{-1}k_x + M_{22}^{-1}k_y = -\frac{\sqrt{3}}{2}k_x - \frac{1}{2}k_y. \end{aligned} \quad (2.6)$$

Both k_x and k_y form a partner set $\beta_1 = \{k_x, k_y\}$ ⁹. In the case of greater powers n of the the transformed tensor elements, there are different basis β_n that need to satisfy the same criteria. For second order polynomials we have to take the power of each transformed element (2.6):

$$C_3^{-1} k_x^2 = (k'_x)^2 = \left(-\frac{1}{2}k_x + \frac{\sqrt{3}}{2}k_y\right)^2 = \left(\frac{k_x^2}{4} - \frac{\sqrt{3}}{2}k_xk_y + \frac{3}{4}k_y^2\right), \quad (2.7)$$

$$C_3^{-1} k_y^2 = (k'_y)^2 = \left(\frac{\sqrt{3}}{2}k_x + \frac{1}{2}k_y\right)^2 = \left(\frac{3}{4}k_x^2 + \frac{\sqrt{3}}{2}k_xk_y + \frac{k_y^2}{4}\right). \quad (2.8)$$

Notice that we cannot propose k_x^2 and k_y^2 as a partner set of Γ_6 , because their transformed counterparts are functions of k_x^2 , k_y^2 and k_xk_y . The latter is outside of the proposed partner set. Now, consider the partner set $\beta_2 = \{-k_x^2 + k_y^2, 2k_xk_y\}$,

and the transformations of each element in β_2 :

$$C_3^{-1} (-k_x^2 + k_y^2) = -\frac{1}{2} (-k_x^2 + k_y^2) + \frac{\sqrt{3}}{2} (2k_x k_y), \quad (2.9)$$

$$C_3^{-1} (2k_x k_y) = -\frac{\sqrt{3}}{2} (-k_x^2 + k_y^2) - \frac{1}{2} (2k_x k_y). \quad (2.10)$$

Both expressions are a linear combination of the elements in β_2 . The same way happens for tensor elements of the third power, which form the partner set $\beta_3 = \{k_x (k_x^2 + k_y^2), k_y (k_x^2 + k_y^2)\}$, which transform accordingly:

$$C_3 [k_x (k_x^2 + k_y^2)] = -\frac{1}{2} [k_x (k_x^2 + k_y^2)] + \frac{\sqrt{3}}{2} [k_y (k_x^2 + k_y^2)], \quad (2.11)$$

$$C_3 [k_y (k_x^2 + k_y^2)] = -\frac{\sqrt{3}}{2} [k_x (k_x^2 + k_y^2)] - \frac{1}{2} [k_y (k_x^2 + k_y^2)]. \quad (2.12)$$

An important observation is that for all basis functions, the C_3^{-1} representation is recovered after each partner set was transformed, and has the form (2.13). Notably, the set of all partner sets β represents the basis functions of irrep Γ_6 , and can be expanded up to an arbitrary order of the polynomials $\beta \equiv \{\beta_1, \beta_2, \beta_3 \dots\}$.

$$\mathcal{R}(C_3^{-1}) = \begin{pmatrix} -\frac{1}{2} & \frac{\sqrt{3}}{2} \\ -\frac{\sqrt{3}}{2} & -\frac{1}{2} \end{pmatrix} \quad (2.13)$$

2.4 Character tables

The Character Table 2.1 for D_{3h} shows both Mulliken and Schoenflies notation for symmetry elements and irreps, respectively. Notice this table gives valuable information. For example, the sum of the number of elements in the group yields the order, or more formally, the cardinality $h \equiv |\mathcal{G}|$ of the group. In the case of D_{3h} , the order is $h = 2 \cdot (1 + 2 + 3) = 12$.

Table 2.1: Character Table for D_{3h} point group and $D_{3h}(M)^2$ double group¹

$D_{3h}(M)^2$	E	E^*	(123)	$(123)^*$	(23)	$(23)^*$	R	$R(123)$	$R(123)^*$
	1	1	2	2	3[6]	3[6]	1	2	2
D_{3h}	E	σ_h	$2C_3$	$2S_3$	$3C'_2$	$3\sigma_v$	—	—	—
Equiv. rot.	R^0	R_z^π	$R_z^{2\pi/3}$	$R_z^{-\pi/3}$	R_0^π	$R_{\pi/2}^\pi$	$R^{2\pi}$	$R_z^{8\pi/3}$	$R_z^{5\pi/3}$
$\Gamma_1 (A_1')$	1	1	1	1	1	1	1	1	1
$\Gamma_2 (A_2')$	1	1	1	1	-1	-1	1	1	1
$\Gamma_3 (A_1'')$	1	-1	1	-1	1	-1	1	1	-1
$\Gamma_4 (A_2'')$	1	-1	1	-1	-1	1	1	1	1
$\Gamma_5 (E'')$	2	-2	-1	1	0	0	2	-1	1
$\Gamma_6 (E')$	2	2	-1	-1	0	0	2	-1	-1
$\Gamma_7 (E_{1/2})$	2	0	1	$\sqrt{3}$	0	0	-2	-1	$-\sqrt{3}$
$\Gamma_8 (E_{3/2})$	2	0	-2	0	0	0	-2	2	0
$\Gamma_9 (E_{5/2})$	2	0	1	$-\sqrt{3}$	0	0	-2	-1	$\sqrt{3}$

Table 2.1 has an extension, when compared to conventional character tables, which includes the elements of the double group. Formally, the double group is defined as $\mathcal{G}_d = \mathcal{G} \oplus \bar{E}\mathcal{G}$, where \bar{E} is a rotation by 2π around an arbitrary axis³, which doubles the order of the group. Irreps Γ_1 through Γ_6 comprise point group D_{3h} . Irreps Γ_1 through Γ_9 make the double group, often referred to as $D_{3h}(M)^2$ ¹.

The rotations for discrete groups are finite and can be defined as generalized unitary rotations $\hat{U}(\phi)$ ¹³. These groups consider the spin degree of freedom in fermionic systems. Generally, a $(2s + 1)$ spinor changes sign under a 2π rotation for fermions. In the case of electrons $s = 1/2$, the unitary direction $\mathbf{n} = \mathbf{z}$ and spin operator $\hat{\mathbf{T}} = \mathbf{S}$, which yields the rotation

$$\hat{U}(\phi = 2\pi) = e^{-i2\pi\mathbf{n}\cdot\hat{\mathbf{T}}/\hbar} = e^{-i\pi\sigma_z} = -\mathbf{1}. \quad (2.14)$$

This represents the fact that spinors change sign under a 2π rotation. However, it is possible to pick a basis that does not change under this rotation. For the D_{3h} point group, this basis transforms according to the irrep Γ_5^3 .

The character $\chi(g)$ of a symmetry element $g \in \mathcal{G}$ is defined as the trace of the matrix representation $\mathcal{D}(g)$ ⁹. Both belong to a particular representation Γ_j :

$$\chi^{(\Gamma_j)}(g) = \text{tr } \mathcal{D}^{(\Gamma_j)}(g) = \sum_{\mu=1}^{\ell_j} \mathcal{D}^{(\Gamma_j)}(g)_{\mu\mu}, \quad (2.15)$$

where ℓ_j is the dimensionality of Γ_j , which will possess h characters, one for each symmetry element. These are invariant under similarity transformations U , therefore providing a systematic way of characterizing point groups, since representations of symmetry elements are not unique.

An important theorem in group theory states that the sum of squares of the dimensions ℓ_j of all irreps Γ_j of a finite group \mathcal{G} equals the order of the group:

$$\sum_j \ell_j^2 = |\mathcal{G}| = h. \quad (2.16)$$

This relation comes in handy when one is trying to find all the irreps of a point group. If there are any missing irreps, Equation (2.16) will not hold. From Table 2.1, the dimension of each representation in D_{3h} is obtained from the identity element column E , since $\chi(E)$ equals the dimension of the matrix. Clearly, this theorem holds, since $4 \cdot 1^2 + 2 \cdot 2^2 = 12$.

One way of obtaining a reducible representation of a point group is using direct products of irreps of the same group. The characters of these representations are enough to characterize them. Let Γ_j and Γ_ℓ be two irreps of \mathcal{G} . The character of the reducible representation $\Gamma_j \otimes \Gamma_\ell$, for each element $g \in \mathcal{G}$, is given by:

$$\chi^{(\Gamma_j \otimes \Gamma_\ell)}(g) = \chi^{(\Gamma_j)}(g) \chi^{(\Gamma_\ell)}(g). \quad (2.17)$$

2.5 Reducible Representations and Hamiltonians

It is possible to express the reduced form of a reducible representation Γ as a linear combination, in direct sum form, of the m irreps Γ_m of \mathcal{G} , as shown in equation (2.18). Additionally, the characters $\chi(g)$ of a reducible representation Γ can also be expanded as a linear combination of the characters of irreps $\chi^{(\Gamma_i)}(g) \forall g \in \mathcal{G}$ with the same a_j coefficients found in the reduction (2.19):

$$\Gamma = a_1 \Gamma_1 \oplus a_2 \Gamma_2 \oplus \cdots \oplus a_m \Gamma_m \quad (2.18)$$

$$\chi(g) = \sum_{\Gamma_j} a_j \chi^{(\Gamma_j)}(g) = a_1 \chi^{(\Gamma_1)}(g) + \cdots + a_m \chi^{(\Gamma_m)}(g). \quad (2.19)$$

The coefficients a_j are defined according to Equation (2.20), a sum over the k classes of D_{3h} , where N_k represents the number of elements of each class. Each coefficient is obtained for one irrep Γ_j . These coefficients also allow us to express a reducible representation as a direct sum of irreps Γ_j .

$$a_j = \frac{1}{h} \sum_k N_k [\chi^{(\Gamma_j)}(g)]^* \chi(g) \quad (2.20)$$

The Hamiltonian matrix is diagonalized by a basis set Φ_μ that transforms according to a representation Γ of the point group \mathcal{G} to which the crystal belongs. A general Hamiltonian \mathcal{H} can be decomposed into blocks $\mathcal{H}_{\alpha\beta}$ ¹², where α and β represent the spaces of the basis functions with a degeneracy n_α and n_β :

$$\mathcal{H}_{\alpha\beta}(\mathcal{K}) = \sum_{\kappa,\lambda} a_{\kappa\lambda}^{\alpha\beta} \sum_{l=1}^{L_\kappa} X_l^{(\kappa)} \mathcal{K}_l^{(\kappa,\lambda)*}, \quad (2.21)$$

and which transforms according to irreps Γ_α and Γ_β of the group \mathcal{G} . Notice this expansion is written in terms of a complete set of linearly independent $n_\alpha \times n_\beta$ matrices $X^{(\kappa)}$ which transform according to the irreps that make up the reducible representation $\Gamma_\alpha \otimes \Gamma_\beta^*$ ³, which can be reduced according to Equation (2.20).

If a block Hamiltonian of the form (2.21) is used, then by the transformation (2.4) we get the rotated Hamiltonian (2.22). Since the expansion is a multiple sum, the matrix products happen for every term in the summation. The tensor elements $\mathcal{K}_l^{(\kappa,\lambda)*}$ are scalar functions, so they can skip the matrix product with $\mathcal{D}^{-1}(g)$. Only the symmetrized matrices $X_l^{(\kappa)}$ are mapped to $X_l'^{(\kappa)}$, as shown.

$$\begin{aligned}
\mathcal{H}'_{\alpha\beta}(\mathcal{K}') &= \mathcal{D}(g) \left\{ \sum_{\kappa,\lambda} a_{\kappa\lambda}^{\alpha\beta} \sum_{l=1}^{L_\kappa} X_l^{(\kappa)} \left[g^{-1} \mathcal{K}'_l^{(\kappa,\lambda)*} \right] \right\} \mathcal{D}^{-1}(g), \\
\mathcal{H}'_{\alpha\beta}(\mathcal{K}') &= \sum_{\kappa,\lambda} a_{\kappa\lambda}^{\alpha\beta} \sum_{l=1}^{L_\kappa} \left\{ \mathcal{D}(g) X_l^{(\kappa)} \mathcal{D}^{-1}(g) \right\} \mathcal{K}'_l^{(\kappa,\lambda)*}, \\
\mathcal{H}'_{\alpha\beta}(\mathcal{K}') &= \sum_{\kappa,\lambda} a_{\kappa\lambda}^{\alpha\beta} \sum_{l=1}^{L_\kappa} X_l^{(\kappa)} \mathcal{K}'_l^{(\kappa,\lambda)*}.
\end{aligned} \tag{2.22}$$

The π electrons on each Dirac valley $\pm\mathbf{K}$ of graphene may be represented by a wave function $\Psi_{\mathbf{K}\lambda}$ which has been projected onto D_{3h} point group, and transforms according to the Γ_5 irrep³, since the tight binding hamiltonian ignores the spin degree of freedom, and this basis will not change sign under a rotation. This allows to define the block Hamiltonian of the form $\mathcal{H}_{55}(\mathcal{K})$, which corresponds to the reducible representation $\Gamma_5 \otimes \Gamma_5^*$. Some reducible representations of D_{3h} are shown in Table 2.2.

Table 2.2: Reducible Direct Products for D_{3h}

D_{3h}	E	σ_h	$2C_3$	$2S_3$	$3C'_2$	$3\sigma_v$	Reduction
$\Gamma_5 \otimes \Gamma_5^*$	4	4	1	1	0	0	$\Gamma_1 \oplus \Gamma_2 \oplus \Gamma_6$
$\Gamma_5 \otimes \Gamma_6^*$	4	-4	1	-1	0	0	$\Gamma_3 \oplus \Gamma_4 \oplus \Gamma_5$
$\Gamma_6 \otimes \Gamma_6^*$	4	4	1	1	0	0	$\Gamma_1 \oplus \Gamma_2 \oplus \Gamma_6$

The expansion of a reducible representation into its irreducible constituents is unique⁹. Therefore, when the characters of two different representations are reduced to the same combination of irreps, such as $\Gamma_5 \otimes \Gamma_5^*$ and $\Gamma_6 \otimes \Gamma_6^*$, the reducible representations are the same, as shown in Table 2.2. We then pick $\Gamma_5 \otimes \Gamma_5^*$ as the non-trivial reducible representation.

To work out the a_j coefficients for $\Gamma_5 \otimes \Gamma_5^*$ in Table 2.1, it is necessary to

pick an irrep Γ_j . Let's pick Γ_6 . Then, characters for the irrep are obtained using Table 2.1, and the characters of the reducible representation are obtained using Equation (2.17), as shown in Table 2.2. To see an example of the reduction of the reducible representation, see Annex E. Finally, according to definition (2.3), the representation consists of 4-dimensional matrices in block form

$$\mathcal{D}^{(\Gamma_5 \otimes \Gamma_5^*)}(g) = \left(\begin{array}{c|c|c} \mathcal{D}^{(\Gamma_1)}(g) & 0 & \mathcal{O} \\ \hline 0 & \mathcal{D}^{(\Gamma_2)}(g) & \mathcal{O} \\ \hline \mathcal{O} & \mathcal{O} & \mathcal{D}^{(\Gamma_6)}(g) \end{array} \right). \quad (2.23)$$

The last detail about the block Hamiltonian (2.21) is that general tensor operators \mathcal{K}_l may depend on the momentum vector \mathbf{k} and external vector fields such as the electric and magnetic fields \mathcal{E} and \mathcal{B} , or spin \mathbf{s} of electrons. It is possible to find tables with tensor elements for each irrep of a point group in polynomial form, to several orders. To obtain them to a desired order, the matrix representations of D_{3h} are used on a coordinate system such as the one shown in Figure 1.1b.

Chapter 3

Results

3.1 Invariant expansion at A and B sublattices

The wave function for π electrons in graphene transforms according to the irrep Γ_5 in the D_{3h} point group³, and as a consequence, the Hamiltonian matrix operator is made of basis functions that transform according to the direct product $\Gamma_5 \otimes \Gamma_5^*$.

Going back to Equation 2.21, the indices for graphene are $\alpha = \beta = 5$, such that the Hamiltonian matrix $\mathcal{H}_{55}^{\mathbf{K}}$ spans over irreps $\kappa = 1, 2, 6$. Notice that the dimension of each irreducible representations are $L_1 = L_2 = 1$, and $L_6 = 2$. The symmetrized matrices $X_l^{(\kappa)}$ for each irrep are $\Gamma_1 : \mathbf{1}$, $\Gamma_2 : \sigma_z$, and $\Gamma_6 : (\sigma_x, \sigma_y)^{3,12}$. The irreducible tensor operators $\mathcal{K}_l^{(\kappa, \lambda)*}$ are dependent on the basis functions to be chosen for the Hamiltonian. The constants then will change accordingly. Table 3.1 summarizes all parameters needed for the expansion.

Table 3.1: Expansion parameters for momentum \mathbf{k} and spin \mathbf{s}

Irrep Γ_κ	Dim. L_κ	Matrices $X_l^{(\kappa)}$	Order λ	Tensors $\mathcal{K}_l^{(\kappa,\lambda)}$
Γ_1	1	$\mathbb{1}$	0, 1, 2	$1 ; k_x^2 + k_y^2 ; (3k_y^2 - k_x^2) k_x$
Γ_2	1	σ_z	1	s_z
Γ_6	2	σ_x, σ_y	1, 2, 3	$k_x, k_y ; k_y^2 - k_x^2, 2k_x k_y ;$ $(k_x^2 + k_y^2) k_x, (k_x^2 + k_y^2) k_y$

An expansion of the $\mathcal{H}_{55}^{\mathbf{K}}$ Hamiltonian matrix, for the A sublattice, on all basis functions λ for any given order is possible using the definition in Equation 3.1. The series is expanded from inside out. A detailed explanation of how the indices work is shown in Annex F.

$$\begin{aligned}
\mathcal{H}_{55}^{\mathbf{K}}(\mathcal{K}) &= \sum_{\kappa,\lambda} a_{\kappa\lambda}^{55} \sum_{l=1}^{L_\kappa} X_l^{(\kappa)} \mathcal{K}_l^{(\kappa,\lambda)*} \quad \text{for } \kappa = 1, 2, 6 \\
\mathcal{H}_{55}^{\mathbf{K}}(\mathcal{K}) &= \sum_{\lambda} \left\{ a_{1\lambda}^{55} X_1^{(1)} \mathcal{K}_1^{(1,\lambda)*} + a_{2\lambda}^{55} X_1^{(2)} \mathcal{K}_1^{(2,\lambda)*} + a_{6\lambda}^{55} \left(X_1^{(6)} \mathcal{K}_1^{(6,\lambda)*} + X_2^{(6)} \mathcal{K}_2^{(6,\lambda)*} \right) \right\} \\
\mathcal{H}_{55}^{\mathbf{K}}(\mathcal{K}) &= \sum_{\lambda} \left\{ a_{1\lambda}^{55} \mathbb{1} \mathcal{K}_1^{(1,\lambda)*} + a_{2\lambda}^{55} \sigma_z \mathcal{K}_1^{(2,\lambda)*} + a_{6\lambda}^{55} \left(\sigma_x \mathcal{K}_1^{(6,\lambda)*} + \sigma_y \mathcal{K}_2^{(6,\lambda)*} \right) \right\}
\end{aligned} \tag{3.1}$$

Notice that Table 3.1 contains only tensor operators with components of the momentum vector \mathbf{k} and the spin s_z operator. These were considered to match the perturbed TB Hamiltonian in equation (1.45). However, it is possible to extend the physical description with other tensors in relevant situations, such as the electric field \mathcal{E} , magnetic field \mathcal{B} , and strain tensor ϵ_{ij} . The irreducible tensor operators that transform according to irreps Γ_1 , Γ_2 , and Γ_6 are shown in Annex E.

To find the Hamiltonian for the wave vector centered at \mathbf{K}' , it is necessary to use (2.4) and recognize the symmetry operation g^{-1} that suits best. Notice that

$\mathbf{K}' = -\mathbf{K}$, so it is just a reflection over the horizontal axis. Using the system of reference in Figure 1.1b, the matrix representation of this operation is the rotation around the y axis, $R(g^{-1}) = R_y$, such that $R_y^{-1}(k_x, k_y) = (-k_x, k_y)$. Also, notice that this rotation preserves both sub-lattices A and B, so the representation $D(g) = \mathbb{1}^3$. This leaves the transformation as

$$\mathcal{H}_{55}^{\mathbf{K}'}(\mathbf{k}) = \mathcal{H}_{55}^{\mathbf{K}}(R_y^{-1}\mathbf{k}). \quad (3.2)$$

However, it is possible to express a Hamiltonian equation for both Dirac valleys, using the parameter $\tau\mathbf{K} = \pm\mathbf{K}$. The parametrization leads to

$$\begin{aligned} \mathcal{H}_{55}^{\tau}(\mathbf{k}) = & a_{10}^{55}\mathbb{1} + a_{61}^{55}(\sigma_x\tau k_x + \sigma_y k_y) + a_{21}^{55}\sigma_z s_z + a_{11}^{55}\mathbb{1}(k_x^2 + k_y^2) \\ & + a_{12}^{55}\mathbb{1}\tau k_x(-k_x^2 + 3k_y^2) + a_{62}^{55}(\sigma_x(-k_x^2 + k_y^2) + 2\sigma_y\tau k_x k_y) \\ & + a_{63}^{55}(\sigma_x\tau k_x(k_x^2 + k_y^2) + \sigma_y k_y(k_x^2 + k_y^2)). \end{aligned} \quad (3.3)$$

Notice that, in contrast to the tight-binding expansion of the Hamiltonian (1.45), the invariant expansion (3.3) contains the extra term $a_{21}^{55}\sigma_z s_z$ related to an intrinsic spin degree of freedom, which is often ignored in the tight-binding models from the start, since the transfer matrices do not explicitly consider the spin degree of freedom. One has to initially write down a Hamiltonian operator using a very well-informed criterion, and often these cases are handled case by case. Although this is the standard procedure, it can be cumbersome, and inexperienced condensed matter physicists might be prone to ignore important details. Group theory allows us to infer the physics of electrons using only the symmetry properties of the crystal and the basis functions which transform accordingly, proving to be

very useful, even to the experienced physicist.

An interesting detail about Hamiltonian (3.3) is its connection to very well known physics. Consider the valley $\tau = 1$. The term depending linearly on momentum can be stated as $a_{61}^{55}(\sigma_x k_x + \sigma_y k_y) \equiv \hbar v \boldsymbol{\sigma} \cdot \mathbf{k}$, where v is the Fermi velocity, and represents the electrons near the Dirac points move as if they are massless particles. The term $a_{21}^{55} \sigma_z s_z$ acts like a mass because it modifies the eigenvalues of the Hamiltonian, making the gap Δ evident, analogous to the energy gap created by a mass term in the Dirac equation. The approximation leads to (3.4) and (3.5).

$$\mathcal{H}_{55}^{\tau}(\mathbf{k}) \approx \epsilon_{2p} \mathbb{1} + \hbar v \boldsymbol{\sigma} \cdot \mathbf{k} + \Delta \sigma_z s_z \quad (3.4)$$

$$E(\mathbf{k}) = \epsilon_{2p} \pm \sqrt{\hbar^2 v^2 k^2 + \Delta^2} \quad (3.5)$$

Other terms can be analyzed in a similar manner. For example, the term $k_x^2 + k_y^2$ gives electrons an effective mass m^* , in the form $\hbar^2 \mathbf{k}^2 (2m^*)^{-1}$. Also higher order terms have common names in literature. For example, cubic terms are known for trigonal warping, which brakes the conical symmetry around the Dirac points and the energy surface starts becoming like a trigonal pyramid¹⁴. Using the TB constants in Annex C, the Hamiltonian including up to trigonal warping is:

$$\mathcal{H}_{55}^{\mathbf{K}}(\mathbf{k}) \approx \epsilon_{2p} \mathbb{1} + \hbar v \boldsymbol{\sigma} \cdot \mathbf{k} + \lambda_{\text{so}} \sigma_z s_z + \frac{\hbar^2 \mathbf{k}^2}{2m^*} + a_{12}^{55} \mathbb{1} k_x (-k_x^2 + 3k_y^2). \quad (3.6)$$

The main disadvantage of this expansion is the lack of knowledge it provides regarding the physical constants $a_{\kappa\lambda}^{\alpha\beta}$ for each term of the Hamiltonian (2.21). This

approach then borrows physical criteria from the tight-binding methods to determine the value of each constant while being consistent with the terms considered in the Hamiltonian. Annex C contains information about all these coefficients.

3.2 *No-go* SOC matrix elements

Pristine graphene naturally belongs to the D_{6h} point group. The subdivision of graphene into two sub-lattices implies a reduction of the symmetry elements to that of D_{3h} , a subgroup of D_{6h} , and as a result both share several symmetry operations. Some of these operations inhibit matrix elements that contribute to the SOC Hamiltonian, according to Kochan's *no-go* rules⁴.

To see these rules, consider the atom notation in Figure 2.1. Also consider a π -orbital state $|X_m\sigma\rangle$ on an m site with a spin degree of freedom $\sigma = \{\uparrow, \downarrow\} \equiv \{+1, -1\}$, in direct space⁴. The first *no-go* rule states that the horizontal reflection σ_h operation inhibits all spin-flip SOC terms⁴, meaning that any matrix element attempting to connect any two sites with spins of different orientations is zero:

$$\langle X_m\sigma | \hat{\mathcal{H}}_{\text{so}} | X_n(-\sigma) \rangle \xrightarrow{\sigma_h} - \langle X_m\sigma | \hat{\mathcal{H}}_{\text{so}} | X_n(-\sigma) \rangle, \quad (3.7)$$

which applies to any pair of m and n sites on the lattice, as shown in Figure 3.1a.

The second *no-go* rule states that the combination of spatial inversion \mathcal{I} , lattice translation $T_{\mathbf{a}}$, and temporal inversion \mathcal{T} inhibits spin-flip SOC terms between first-nearest neighbors, that is, between neighboring atoms of different sublattices⁴. The

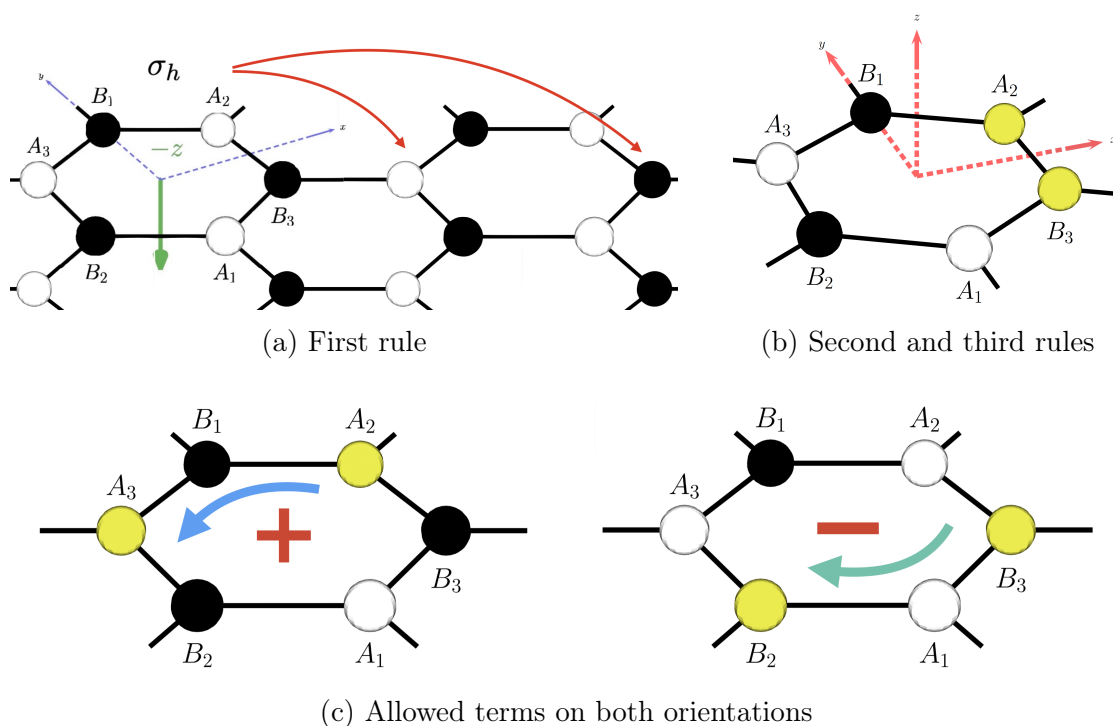


Figure 3.1: Diagrams for *no-go* rules. Notice that the first rule at (a) applies for any pair of sites on the lattice. The second and third rules (b) only consider the first-nearest neighbors.

matrix elements as in Figure 3.1b are:

$$\begin{aligned}
 \langle A_2\sigma | \hat{\mathcal{H}}_{\text{so}} | B_3(-\sigma) \rangle &\xrightarrow{\mathcal{I}} \langle B_2\sigma | \hat{\mathcal{H}}_{\text{so}} | A_3(-\sigma) \rangle, \\
 \langle B_2\sigma | \hat{\mathcal{H}}_{\text{so}} | A_3(-\sigma) \rangle &\xrightarrow{T_{\mathbf{a}}} \langle B_3\sigma | \hat{\mathcal{H}}_{\text{so}} | A_2(-\sigma) \rangle, \\
 \langle B_3\sigma | \hat{\mathcal{H}}_{\text{so}} | A_2(-\sigma) \rangle &\xrightarrow{\mathcal{T}} -\langle A_2\sigma | \hat{\mathcal{H}}_{\text{so}} | B_3(-\sigma) \rangle.
 \end{aligned} \tag{3.8}$$

The third *no-go* rule states that the combination of lattice translation $T_{\mathbf{a}}$ and vertical reflection $3C_2$ inhibits spin-conserving SOC terms between the first-nearest

neighbors⁴. The matrix elements also follow the interaction shown in Figure 3.1b:

$$\begin{aligned} \langle A_2\sigma | \hat{\mathcal{H}}_{\text{so}} | B_3\sigma \rangle &\xrightarrow{T_a} \langle A_3\sigma | \hat{\mathcal{H}}_{\text{so}} | B_2\sigma \rangle, \\ \langle A_3\sigma | \hat{\mathcal{H}}_{\text{so}} | B_2\sigma \rangle &\xrightarrow{3C_2} -\langle A_2\sigma | \hat{\mathcal{H}}_{\text{so}} | B_3\sigma \rangle. \end{aligned} \quad (3.9)$$

The only allowed matrix elements by all operations in D_{3h} are given by:

$$\langle X_m\sigma | \hat{\mathcal{H}}_{\text{so}} | X_n\sigma \rangle = v_{m,n} [\hat{s}_z]_{\sigma\sigma} \frac{i\lambda_1}{3\sqrt{3}}, \quad \text{for } [\hat{s}_z]_{\pm\pm} = \pm 1. \quad (3.10)$$

where λ_1 is the SOC hopping constant found also in the block Hamiltonian (3.3) in the term $a_{21}^{55}\sigma_z s_z$. These allow spin-conserving interactions between second neighbors. This does two things for our model. First, it confirms that it is consistent with the symmetries of the D_{3h} point group. Second, it connects the invariant expansion to matrix elements, as shown in equation (3.11), which as shown in Figure 3.1c, has a dependence on orientation of the hopping, which is negative for clockwise direction and positive for anti-clockwise direction.

$$\frac{i\lambda_1}{3\sqrt{3}} = \langle A_3 \uparrow | \hat{H}_{\text{so}} | A_2 \uparrow \rangle = \langle B_2 \downarrow | \hat{H}_{\text{so}} | B_3 \downarrow \rangle = -\langle B_2 \uparrow | \hat{H}_{\text{so}} | B_3 \uparrow \rangle \quad (3.11)$$

3.3 Software Development

A Python self-contained software that automates the generation of block Hamiltonians of the form (2.21) was created. This software uses the Numpy¹⁵ numeric module and Sympy¹⁶ symbolic computation module to operate. A flowchart that

describes the use of the software is illustrated in Figure 3.2.

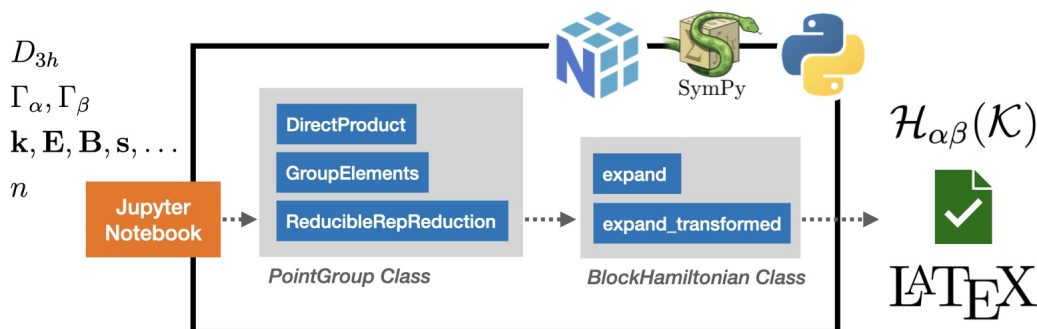


Figure 3.2: Flow chart for the use of the software to generate an invariant expansion of a Hamiltonian operator, using group theory.

The user provides information about a point group, one reducible representation (the block indices), and an appropriate set of tensor operators which describe the physics of the problem. These are passed to an instance of the *BlockHamiltonian* object. This object utilizes the *PointGroup* class for group theory operations, such as obtaining the reducible representation $\Gamma_{\alpha,\beta}$ in terms of irreps, using (2.20).

The *expand* method of the *BlockHamiltonian* class allows the Hamiltonian $\mathcal{H}_{\alpha\beta}$ to be written down to the desired order. The Hamiltonian $\mathcal{H}_{\alpha\beta}$ can be expanded directly or by using transformed basis functions $g\mathcal{K}$ according to a symmetry operation of the group related to the reducible representation. In Annex G, UML diagrams of the classes and the code have been included for reference.

Chapter 4

Conclusions

In this thesis, we developed software using group theory to study quantum operators in materials like graphene. This software handles complex calculations and uses the invariant expansion method to systematically generate Hamiltonians to a desired order by using crystal symmetries, avoiding the exclusion of relevant terms and improving on traditional tight-binding models. The software offers a user-friendly interface for calculating properties of point groups, such as reducible representations and relevant tensor operators. The software outputs the expanded Hamiltonian to the desired order, streamlining the research process.

We demonstrated that group theory ensures all relevant physical terms are considered, based on the crystal's symmetry properties. The invariant expansion method systematically includes all possible physical interactions dictated by crystal symmetries, providing a more accurate description of materials. Using invariant expansion, we identified appropriate basis functions that transform according to

the irreps of the point group D_{3h} , allowing us to expand the Hamiltonian to the desired order while maintaining consistency with crystal symmetries.

For spin-orbit coupling (SOC), the invariant expansion method identified SOC terms consistent with D_{3h} symmetries, including spin-conserving interactions between second neighbors. These terms were validated against Kochan's *no-go* rules, confirming their consistency with known physical constraints.

While this work focused on graphene, the developed methods are generalizable to other two-dimensional materials, opening possibilities for studying other symmetry properties. Future research should develop methods to generate tensor operators for any system and order, enhancing the invariant expansion method's applicability to a broader range of materials and physical systems. This work provides a strong foundation for future studies, offering a systematic and comprehensive approach to modeling and understanding complex material systems.

Bibliography

- [1] Philip Bunker. *Molecular Symmetry and Spectroscopy*. Elsevier Science, Burlington, 1979. OCLC: 843187746.
- [2] M. Gmitra, S. Konschuh, C. Ertler, C. Ambrosch-Draxl, and J. Fabian. Band-structure topologies of graphene: Spin-orbit coupling effects from first principles. *Physical Review B*, 80(23):235431, December 2009.
- [3] R. Winkler and U. Zülicke. Invariant expansion for the trigonal band structure of graphene. *Physical Review B*, 82(24):245313, December 2010.
- [4] Denis Kochan, Susanne Irmer, and Jaroslav Fabian. Model spin-orbit coupling Hamiltonians for graphene systems. *Physical Review B*, 95(16):165415, April 2017.
- [5] F Geissler, J C Budich, and B Trauzettel. Group theoretical and topological analysis of the quantum spin Hall effect in silicene. *New Journal of Physics*, 15(8):085030, August 2013.
- [6] R Saito, G Dresselhaus, and M S Dresselhaus. *Physical Properties of Carbon Nanotubes*. Published by Imperial College Press and distributed by World Scientific Publishing Co., July 1998.

- [7] Edward McCann. Electronic Properties of Monolayer and Bilayer Graphene. In Hassan Raza, editor, *Graphene Nanoelectronics*, pages 237–275. Springer Berlin Heidelberg, Berlin, Heidelberg, 2011.
- [8] Akira Suzuki, Masashi Tanabe, and Shigeji Fujita. Electronic Band Structure of Graphene Based on the Rectangular 4-Atom Unit Cell. *Journal of Modern Physics*, 08(04):607–621, 2017.
- [9] Mildred Dresselhaus, Gene Dresselhaus, Stephen Cronin, and Antonio Gomes Souza Filho. *Solid State Properties*. Graduate Texts in Physics. Springer Berlin Heidelberg, Berlin, Heidelberg, 2018.
- [10] Sergej Konschuh, Martin Gmitra, and Jaroslav Fabian. Tight-binding theory of the spin-orbit coupling in graphene. *Physical Review B*, 82(24):245412, December 2010.
- [11] Marcin Kurpas, Paulo E. Faria Junior, Martin Gmitra, and Jaroslav Fabian. Spin-orbit coupling in elemental two-dimensional materials. *Physical Review B*, 100(12):125422, September 2019.
- [12] Gennadii Levikovich Bir and Grigorii Ezekievich Pikus. *Symmetry and strain-induced effects in semiconductors*. Wiley, New York, 1974.
- [13] Nouredine Zettili. *Quantum mechanics: concepts and applications*. Wiley, Chichester, U.K, 2nd ed edition, 2009. OCLC: ocn255894625.
- [14] K. Kechedzhi, Vladimir I. Fal’ko, E. McCann, and B. L. Altshuler. Influence of Trigonal Warping on Interference Effects in Bilayer Graphene. *Physical Review Letters*, 98(17):176806, April 2007.

- [15] Charles R. Harris, K. Jarrod Millman, Stéfan J. Van Der Walt, Ralf Gommers, Pauli Virtanen, David Cournapeau, Eric Wieser, Julian Taylor, Sebastian Berg, Nathaniel J. Smith, Robert Kern, Matti Picus, Stephan Hoyer, Marten H. Van Kerkwijk, Matthew Brett, Allan Haldane, Jaime Fernández Del Río, Mark Wiebe, Pearu Peterson, Pierre Gérard-Marchant, Kevin Sheppard, Tyler Reddy, Warren Weckesser, Hameer Abbasi, Christoph Gohlke, and Travis E. Oliphant. Array programming with NumPy. *Nature*, 585(7825):357–362, September 2020.
- [16] Aaron Meurer, Christopher P. Smith, Mateusz Paprocki, Ondřej Čertík, Sergey B. Kirpichev, Matthew Rocklin, AMiT Kumar, Sergiu Ivanov, Jason K. Moore, Sartaj Singh, Thilina Rathnayake, Sean Vig, Brian E. Granger, Richard P. Muller, Francesco Bonazzi, Harsh Gupta, Shivam Vats, Fredrik Johansson, Fabian Pedregosa, Matthew J. Curry, Andy R. Terrel, Štěpán Roučka, Ashutosh Saboo, Isuru Fernando, Sumith Kulal, Robert Cimrman, and Anthony Scopatz. SymPy: symbolic computing in Python. *PeerJ Computer Science*, 3:e103, January 2017.

Chapter 5

Annexes

Annex A: Nearest neighbors on graphene

The nearest-neighbors in the basis $\hat{\mathbf{x}}, \hat{\mathbf{y}}$; where obtained graphically from Figure 1.2. When a B atom is used as the reference, the first three $\boldsymbol{\tau}_1^{(j)}$ nearest-neighbors are A atoms, so involve inter-lattice hopping of electrons. These vectors are:

$$\boldsymbol{\tau}_1^{(1)} = \begin{pmatrix} -\frac{a}{2} \\ -\frac{\sqrt{3}a}{6} \end{pmatrix}, \quad \boldsymbol{\tau}_1^{(2)} = \begin{pmatrix} \frac{a}{2} \\ -\frac{\sqrt{3}a}{6} \end{pmatrix}, \quad \boldsymbol{\tau}_1^{(3)} = \begin{pmatrix} 0 \\ \frac{\sqrt{3}a}{3} \end{pmatrix}.$$

There are six second, or next-nearest neighbors $\boldsymbol{\tau}_2^{(j)}$. These describe intra-

lattice movement of electrons B-B. The first three next nearest-neighbors are:

$$\boldsymbol{\tau}_2^{(1)} = \begin{pmatrix} \frac{a}{2} \\ \frac{\sqrt{3}a}{2} \end{pmatrix}, \quad \boldsymbol{\tau}_2^{(2)} = \begin{pmatrix} -\frac{a}{2} \\ \frac{\sqrt{3}a}{2} \end{pmatrix}, \quad \boldsymbol{\tau}_2^{(3)} = \begin{pmatrix} -a \\ 0 \end{pmatrix}.$$

The remaining vectors satisfy the following relations: $\boldsymbol{\tau}_2^{(4)} = -\boldsymbol{\tau}_2^{(1)}$, $\boldsymbol{\tau}_2^{(5)} = -\boldsymbol{\tau}_2^{(2)}$, and $\boldsymbol{\tau}_2^{(6)} = -\boldsymbol{\tau}_2^{(3)}$. These can be verified in Figure 1.2b. Finally, the third or next next-nearest neighbors $\boldsymbol{\tau}_3^{(j)}$ are again, inter-lattice electron mobility B-A, and are the following, as seen in Figure 1.2c:

$$\boldsymbol{\tau}_3^{(1)} = \begin{pmatrix} a \\ \frac{\sqrt{3}a}{3} \end{pmatrix}, \quad \boldsymbol{\tau}_3^{(2)} = \begin{pmatrix} -a \\ \frac{\sqrt{3}a}{3} \end{pmatrix}, \quad \boldsymbol{\tau}_3^{(3)} = \begin{pmatrix} 0 \\ -\frac{2\sqrt{3}a}{3} \end{pmatrix}.$$

It is possible to find more k -nearest neighbors to any arbitrary number k , however it would depend on each case, since usually beyond the second nearest neighbors, calculations do not add much more precision.

Annex B: Eigenvectors for Graphene

The eigenvectors $\boldsymbol{\psi}_+ = (\psi_+^{(1)}, \psi_+^{(2)})$ and $\boldsymbol{\psi}_- = (\psi_-^{(1)}, \psi_-^{(2)})$. Since there is always one free variable, I pick a value that normalizes the wavefunction.

$$\begin{aligned}
n = +1 : \left(\begin{array}{cc|c} -t_1|f| & t_1f & 0 \\ t_1f^* & -t_1|f| & 0 \end{array} \right) &\sim \left(\begin{array}{cc|c} -ff^* & f|f| & 0 \\ f^*|f| & -ff^* & 0 \end{array} \right) \\
&\sim \left(\begin{array}{cc|c} -ff^*f^* & ff^*|f| & 0 \\ ff^*f^* & -ff^*|f| & 0 \end{array} \right) \sim \left(\begin{array}{cc|c} -ff^*f^* & ff^*|f| & 0 \\ 0 & (f-f^*)f^*|f| & 0 \end{array} \right) \\
&\sim \left(\begin{array}{cc|c} -\hat{f}^* & 1 & 0 \\ 0 & 0 & 0 \end{array} \right) \implies \psi_+^{(2)} = \hat{f}^* \psi_+^{(1)}
\end{aligned}$$

$$\begin{aligned}
n = -1 : \left(\begin{array}{cc|c} t_1|f| & t_1f & 0 \\ t_1f^* & t_1|f| & 0 \end{array} \right) &\sim \left(\begin{array}{cc|c} ff^* & f|f| & 0 \\ f^*|f| & ff^* & 0 \end{array} \right) \\
&\sim \left(\begin{array}{cc|c} ff^*|f| & fff^* & 0 \\ ff^*|f| & fff^* & 0 \end{array} \right) \sim \left(\begin{array}{cc|c} ff^*|f| & fff^* & 0 \\ (f-f)f^*|f| & 0 & 0 \end{array} \right) \\
&\sim \left(\begin{array}{cc|c} 1 & \hat{f} & 0 \\ 0 & 0 & 0 \end{array} \right) \implies \psi_-^{(1)} = -\hat{f} \psi_-^{(2)}
\end{aligned}$$

Annex C: Physical constants for TB and SOC block Hamiltonian

The series expansion of the TB Hamiltonian matrix elements around the Dirac point \mathbf{K} contains several coefficients has the form:

$$\begin{aligned}
 \mathcal{H}_{\lambda\lambda} &= \epsilon_{2p} + \frac{3}{4}a^2t_2(k_x^2 + k_y^2) + \frac{\sqrt{3}}{8}a^3t_2k_x[-k_x^2 + 3k_y^2], \\
 \mathcal{H}_{AB} &= a\left(-\frac{\sqrt{3}t_1}{2} + \sqrt{3}t_3\right)[k_x + ik_y] \\
 &\quad + a^2\left(\frac{t_1}{8} + \frac{t_3}{2}\right)[(k_x^2 - k_y^2) - 2ik_xk_y] \\
 &\quad + a^3\left(\frac{\sqrt{3}t_1}{48} - \frac{\sqrt{3}t_3}{6}\right)[k_x(k_x^2 + k_y^2) + ik_y(k_x^2 + k_y^2)].
 \end{aligned} \tag{5.1}$$

where there are imaginary components, that when factored out from the complete matrix form, transform into Pauli matrices. Refer to equations (1.45) and (3.3) to compare both Hamiltonians using these constants and verify both are the same.

$$a_{10}^{55} = \epsilon_{2p} \tag{5.2a} \qquad a_{61}^{55} = a\left(-\frac{\sqrt{3}t_1}{2} + \sqrt{3}t_3\right) \tag{5.2e}$$

$$a_{11}^{55} = \frac{3}{4}a^2t_2 \tag{5.2b} \qquad a_{62}^{55} = a^2\left(\frac{t_1}{8} + \frac{t_3}{2}\right) \tag{5.2f}$$

$$a_{12}^{55} = \frac{\sqrt{3}}{8}a^3t_2 \tag{5.2c} \qquad a_{63}^{55} = a^3\left(\frac{\sqrt{3}t_1}{48} - \frac{\sqrt{3}t_3}{6}\right) \tag{5.2g}$$

$$a_{21}^{55} = \frac{3}{2}\lambda_{\text{so}}a^2 \tag{5.2d}$$

Annex D: Matrix representations for symmetry elements in D_{3h}

Table 5.1: Matrix representations for elements in D_{3h}

Class k	Element g	Matrix representations $\mathcal{D}(g)$ on orthonormal vector basis
1	E	$\begin{pmatrix} 1 & 0 & 0 \\ 0 & 1 & 0 \\ 0 & 0 & 1 \end{pmatrix}$
2	σ_h	$\begin{pmatrix} 1 & 0 & 0 \\ 0 & 1 & 0 \\ 0 & 0 & -1 \end{pmatrix}$
3	C_3 C_3^{-1}	$\begin{pmatrix} -\frac{1}{2} & \frac{\sqrt{3}}{2} & 0 \\ -\frac{\sqrt{3}}{2} & -\frac{1}{2} & 0 \\ 0 & 0 & 1 \end{pmatrix}, \begin{pmatrix} -\frac{1}{2} & -\frac{\sqrt{3}}{2} & 0 \\ \frac{\sqrt{3}}{2} & -\frac{1}{2} & 0 \\ 0 & 0 & 1 \end{pmatrix}$
4	S_3 S_3^{-1}	$\begin{pmatrix} -\frac{1}{2} & \frac{\sqrt{3}}{2} & 0 \\ -\frac{\sqrt{3}}{2} & -\frac{1}{2} & 0 \\ 0 & 0 & -1 \end{pmatrix}, \begin{pmatrix} -\frac{1}{2} & -\frac{\sqrt{3}}{2} & 0 \\ \frac{\sqrt{3}}{2} & -\frac{1}{2} & 0 \\ 0 & 0 & -1 \end{pmatrix}$
5	$C'_{2,1}$ $C'_{2,2}$ $C'_{2,3}$	$\begin{pmatrix} -\frac{1}{2} & -\frac{\sqrt{3}}{2} & 0 \\ -\frac{\sqrt{3}}{2} & \frac{1}{2} & 0 \\ 0 & 0 & -1 \end{pmatrix}, \begin{pmatrix} -1 & 0 & 0 \\ 0 & 1 & 0 \\ 0 & 0 & -1 \end{pmatrix}, \begin{pmatrix} -\frac{1}{2} & \frac{\sqrt{3}}{2} & 0 \\ \frac{\sqrt{3}}{2} & \frac{1}{2} & 0 \\ 0 & 0 & -1 \end{pmatrix}$
6	$\sigma_{v,1}$ $\sigma_{v,2}$ $\sigma_{v,3}$	$\begin{pmatrix} -\frac{1}{2} & -\frac{\sqrt{3}}{2} & 0 \\ -\frac{\sqrt{3}}{2} & \frac{1}{2} & 0 \\ 0 & 0 & 1 \end{pmatrix}, \begin{pmatrix} -1 & 0 & 0 \\ 0 & 1 & 0 \\ 0 & 0 & 1 \end{pmatrix}, \begin{pmatrix} -\frac{1}{2} & \frac{\sqrt{3}}{2} & 0 \\ \frac{\sqrt{3}}{2} & \frac{1}{2} & 0 \\ 0 & 0 & 1 \end{pmatrix}$

Annex E: Reduction of $\Gamma_5 \otimes \Gamma_5^*$

Let classes E , σ_h , $2C_3$, $2S_3$, $3C_2'$ and $3\sigma_v$ be numbered $k = 1, \dots, 6$, respectively. Let the a_6 coefficient be the scalar on the reduction related to irrep Γ_6 . This coefficient is obtained using equation (2.20) as shown:

$$a_6 = \frac{1}{12} \sum_{k=1}^6 N_k [\chi^{(\Gamma_6)}(g)]^* \chi(g),$$

$$a_6 = \frac{1}{12} [1 \cdot 2 \cdot 4 + 1 \cdot 2 \cdot 4 + 2 \cdot (-1) \cdot 1 + 2 \cdot (-1) \cdot 1 + 3 \cdot 0 \cdot 0 + 3 \cdot 0 \cdot 0],$$

$$a_6 = \frac{8 + 8 - 2 - 2}{12} = \frac{12}{12} = 1.$$

The remaining coefficients are obtained similarly, and are $a_1 = a_2 = 1$, and $a_3 = a_4 = a_5 = 0$, resulting in the reduction $\Gamma_5 \otimes \Gamma_5^* = \Gamma_1 \oplus \Gamma_2 \oplus \Gamma_6$. The complete set of characters for all representations involved in the reduction are in Table 5.2.

Table 5.2: Reducción de representación $\Gamma_5 \otimes \Gamma_5^*$

D_{3h}	E	σ_h	$2C_3$	$2S_3$	$3C_2'$	$3\sigma_v$
$\Gamma_1 (A_1')$	1	1	1	1	1	1
$\Gamma_2 (A_2')$	1	1	1	1	-1	-1
$\Gamma_6 (E')$	2	2	-1	-1	0	0
$\Gamma_5 (E'')$	2	-2	-1	1	0	0
$\Gamma_5 \otimes \Gamma_5^*$	4	4	1	1	0	0

Annex F: Invariant expansion details

Equation (3.1) describes the expansion of the block Hamiltonian \mathcal{H}_{55} . To visualize how the indices are used, the following scheme was crafted. Notice that unidimensional irreps Γ_1 and Γ_2 show only one function on each constant $a_{\kappa\lambda}^{55}$. The irrep Γ_6 is two-dimensional, therefore each constant $a_{\kappa\lambda}^{55}$ is followed by a combination of two tensor operators. These are partner functions.

$$\begin{array}{ccc}
 \Gamma_1 & \Gamma_2 & \Gamma_6 \\
 L_1 = 1 & L_2 = 1 & L_6 = 2 \\
 \underbrace{\hspace{2cm}} & \underbrace{\hspace{2cm}} & \underbrace{\hspace{4cm}} \\
 \mathcal{H}_{55}^{\mathbf{K}} = \sum_{\lambda} \left\{ a_{1\lambda}^{55} \mathcal{X}_1^{(1)} \mathcal{K}_1^{(1,\lambda)*} + a_{2\lambda}^{55} \mathcal{X}_1^{(2)} \mathcal{K}_1^{(2,\lambda)*} + a_{6\lambda}^{55} \left(\mathcal{X}_1^{(6)} \mathcal{K}_1^{(6,\lambda)*} + \mathcal{X}_2^{(6)} \mathcal{K}_2^{(6,\lambda)*} \right) \right\} \\
 \mathcal{H}_{55}^{\mathbf{K}} = \sum_{\lambda} \left\{ a_{1\lambda}^{55} \mathbb{1} \mathcal{K}_1^{(1,\lambda)*} + a_{2\lambda}^{55} \sigma_z \mathcal{K}_1^{(2,\lambda)*} + a_{6\lambda}^{55} \left(\sigma_x \mathcal{K}_1^{(6,\lambda)*} + \sigma_y \mathcal{K}_2^{(6,\lambda)*} \right) \right\}
 \end{array}$$

When using only functions in Table 3.1, the expansion of the Hamiltonian takes the following form, where the order index λ is expanded from the smallest order for each irrep Γ_{κ} :

$$\begin{array}{ccc}
 \Gamma_1 & & \Gamma_2 \\
 \lambda = 0, 1, 2 & & \lambda = 1 \\
 \downarrow & & \downarrow \\
 \mathcal{H}_{55}^{\tau}(\mathbf{k}) = a_{10}^{55} \mathbb{1} + a_{11}^{55} \mathbb{1} (k_x^2 + k_y^2) + a_{12}^{55} \tau k_x (-k_x^2 + 3k_y^2) + a_{21}^{55} \sigma_z s_z \\
 \Gamma_6 \rightarrow + a_{61}^{55} (\sigma_x \tau k_x + \sigma_y k_y) + a_{62}^{55} [\sigma_x (-k_x^2 + k_y^2) + \sigma_y \tau (2k_x k_y)] \\
 \lambda = 1, 2, 3 + a_{63}^{55} [\sigma_x \tau k_x (k_x^2 + k_y^2) + \sigma_y k_y (k_x^2 + k_y^2)].
 \end{array}$$

If there is any other physical scenario, many other basis functions can be chosen, such as the electric field \mathcal{E} , magnetic field \mathcal{B} , and strain tensor ϵ_{ij} . These basis functions for the $\Gamma_5 \otimes \Gamma_5^*$ is shown in Equation (5.3)³.

$$\begin{aligned}
\Gamma_1 : & \quad 1; \quad k_x^2 + k_y^2; \quad (3k_y^2 - k_x^2) k_x; \quad k_x \mathcal{E}_x + k_y \mathcal{E}_y; \quad \epsilon_{xx} + \epsilon_{yy}; \\
& \quad (\epsilon_{yy} - \epsilon_{xx}) k_x + 2\epsilon_{xy} k_y; \quad (\epsilon_{yy} - \epsilon_{xx}) \mathcal{E}_x + 2\epsilon_{xy} \mathcal{E}_y; \\
& \quad s_x \mathcal{B}_x + s_y \mathcal{B}_y; \quad s_z \mathcal{B}_z; \quad (s_x k_y - s_y k_x) \mathcal{E}_z; \quad s_z (k_x \mathcal{E}_y - k_y \mathcal{E}_x) \\
\Gamma_2 : & \quad (3k_x^2 - k_y^2) k_y; \quad \mathcal{B}_z; \quad k_x \mathcal{E}_y - k_y \mathcal{E}_x; \quad (\epsilon_{xx} - \epsilon_{yy}) k_y + 2\epsilon_{xy} k_x; \\
& \quad (\epsilon_{xx} + \epsilon_{yy}) \mathcal{B}_z; \quad (\epsilon_{xx} - \epsilon_{yy}) \mathcal{E}_y + 2\epsilon_{xy} \mathcal{E}_x; \quad s_z; \\
& \quad s_x \mathcal{B}_y - s_y \mathcal{B}_x; \quad (s_x k_x + s_y k_y) \mathcal{E}_z; \quad s_z (\epsilon_{xx} + \epsilon_{yy}) \\
\Gamma_6 : & \quad k_x, k_y; \quad k_y^2 - k_x^2, 2k_x k_y; \quad (k_x^2 + k_y^2) k_x, (k_x^2 + k_y^2) k_y; \\
& \quad \mathcal{B}_z k_y, -\mathcal{B}_z k_x; \quad \mathcal{E}_x, \mathcal{E}_y; \quad k_y \mathcal{E}_y - k_x \mathcal{E}_x, k_x \mathcal{E}_y + k_y \mathcal{E}_x; \\
& \quad \mathcal{E}_y \mathcal{B}_z, -\mathcal{E}_x \mathcal{B}_z; \quad \mathcal{E}_z \mathcal{B}_y, -\mathcal{E}_z \mathcal{B}_x \\
& \quad \epsilon_{yy} - \epsilon_{xx}, 2\epsilon_{xy}; \quad (\epsilon_{xx} + \epsilon_{yy}) (k_x, k_y); \\
& \quad (\epsilon_{xx} - \epsilon_{yy}) k_x + 2\epsilon_{xy} k_y, (\epsilon_{yy} - \epsilon_{xx}) k_y + 2\epsilon_{xy} k_x; \\
& \quad 2\epsilon_{xy} \mathcal{B}_z, (\epsilon_{xx} - \epsilon_{yy}) \mathcal{B}_z; \\
& \quad (\epsilon_{xx} - \epsilon_{yy}) \mathcal{E}_x + \epsilon_{xy} \mathcal{E}_y, (\epsilon_{yy} - \epsilon_{xx}) \mathcal{E}_y + \epsilon_{xy} \mathcal{E}_x; \\
& \quad (\epsilon_{xx} + \epsilon_{yy}) (\mathcal{E}_x, \mathcal{E}_y); \quad s_z k_y, -s_z k_x; \\
& \quad s_y \mathcal{B}_y - s_x \mathcal{B}_x, s_x \mathcal{B}_y + s_y \mathcal{B}_x; \quad s_z \mathcal{E}_y, -s_z \mathcal{E}_x; \\
& \quad s_y \mathcal{E}_z, -s_x \mathcal{E}_z; \quad s_z (k_x \mathcal{E}_y + k_y \mathcal{E}_x), s_z (k_x \mathcal{E}_x - k_y \mathcal{E}_y); \\
& \quad (s_x k_y + s_y k_x) \mathcal{E}_z, (s_x k_x - s_y k_y) \mathcal{E}_z; \quad 2s_z \epsilon_{xy}, s_z (\epsilon_{xx} - \epsilon_{yy});
\end{aligned} \tag{5.3}$$

Annex G: Code for analytic calculations

Both UML diagrams were created using RedDress-PlantUML templates.

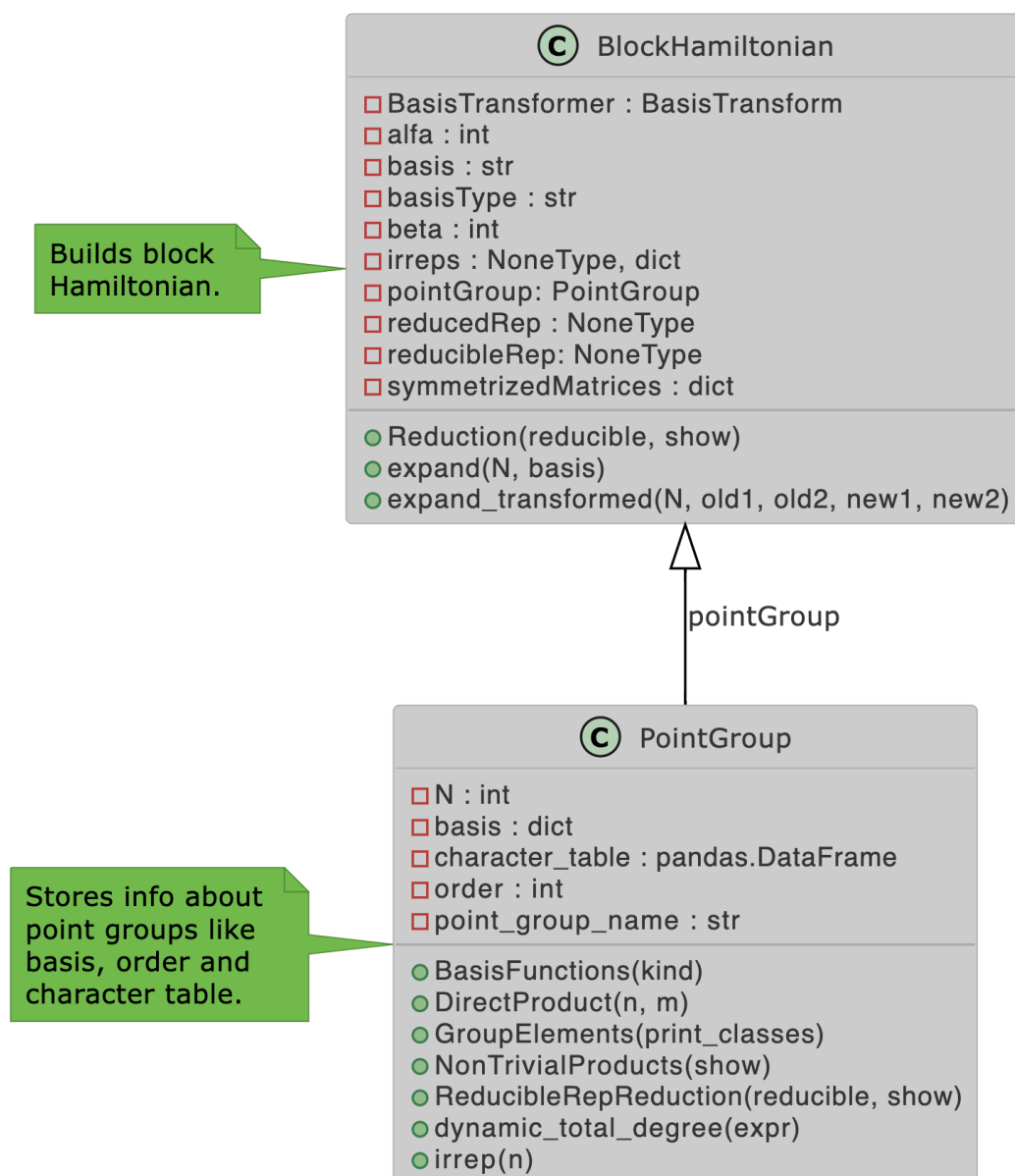


Figure 5.1: UML diagram for *BlockHamiltonian* and *PointGroup* classes.

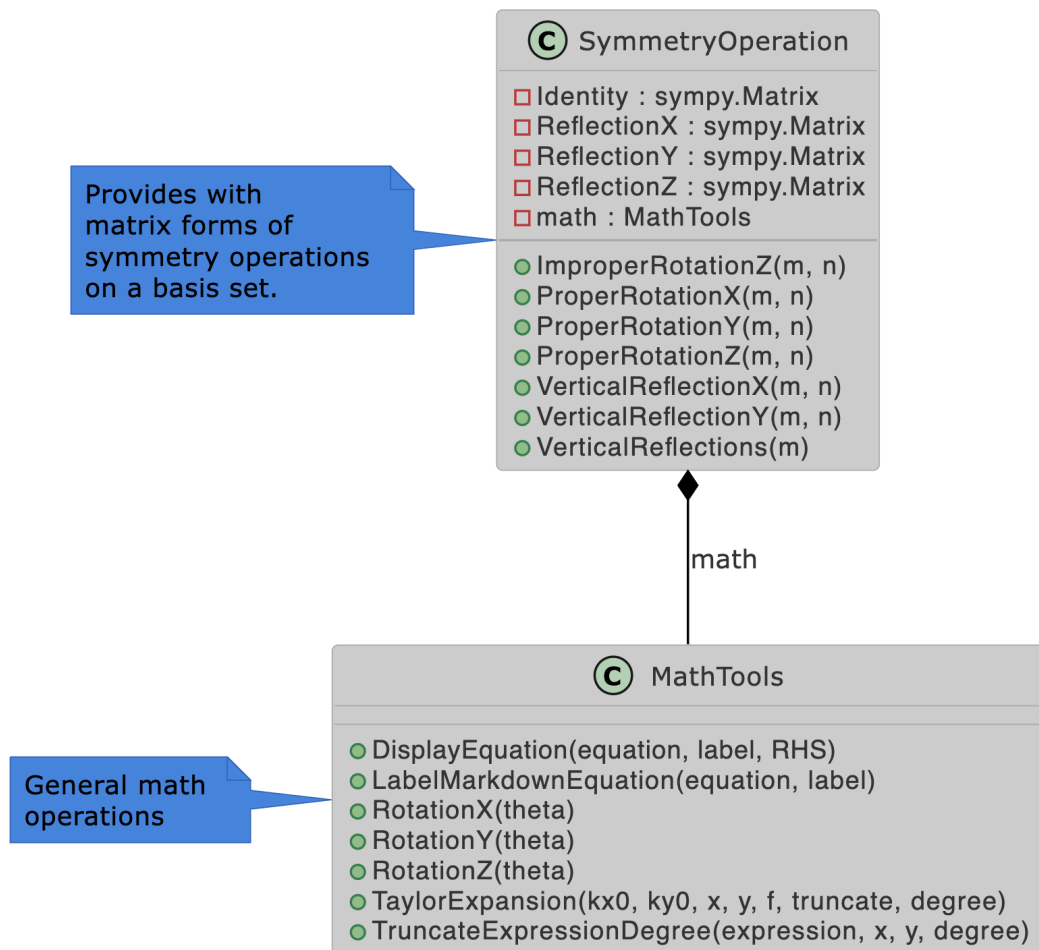


Figure 5.2: UML diagram for *SymmetryOperation* and *MathTools* classes.